

Asymptomatic Infection of Marburg Virus Reservoir Bats Is Explained by a Strategy of Immunoprotective Disease Tolerance

Highlights

- CD14⁺ monocytes show Marburg virus replication after infection of reservoir bats
- Infected bat monocytes and tissues show canonical antiviral response gene induction
- Infected bat host response lacks significant induction of immunopathogenic genes
- Immunoprotective bat response contrasts starkly to that reported for sick primates

Authors

Jonathan C. Guito, Joseph B. Prescott, Catherine E. Arnold, ..., Gustavo F. Palacios, Mariano Sanchez-Lockhart, Jonathan S. Towner

Correspondence

jit8@cdc.gov (J.S.T.),
mariano.sanchez-lockhart.ctr@mail.mil (M.S.-L.)

In Brief

A long-standing question for zoonotic diseases is how animal reservoirs such as bats immunologically control infection by pathogens that often kill spillover hosts such as humans. Guito et al. present clear evidence that Marburg virus-infected Egyptian rousette bats avert pathology by limiting induction of proinflammatory genes linked to severe disease.



Article

Asymptomatic Infection of Marburg Virus Reservoir Bats Is Explained by a Strategy of Immunoprotective Disease Tolerance

Jonathan C. Guito,¹ Joseph B. Prescott,² Catherine E. Arnold,³ Brian R. Amman,¹ Amy J. Schuh,¹ Jessica R. Spengler,¹ Tara K. Sealy,¹ Jessica R. Harmon,¹ JoAnn D. Coleman-McCray,¹ Kirsten A. Kulcsar,⁴ Elyse R. Nagle,⁵ Raina Kumar,⁵ Gustavo F. Palacios,⁵ Mariano Sanchez-Lockhart,^{5,6,*} and Jonathan S. Towner^{1,7,8,*}

¹Viral Special Pathogens Branch, Centers for Disease Control and Prevention, Atlanta, GA 30329, USA

²Center for Biological Threats and Special Pathogens, Robert Koch Institute, Berlin, Germany

³Diagnostic Systems Division, U.S. Army Medical Research Institute of Infectious Diseases (USAMRIID), Fort Detrick, MD 21702, USA

⁴Department of Microbiology and Immunology, University of Maryland School of Medicine, Baltimore, MD 21201, USA

⁵Center for Genome Sciences, USAMRIID, Fort Detrick, MD 21702, USA

⁶Department of Pathology and Microbiology, University of Nebraska Medical Center, Omaha, NE 68198, USA

⁷Department of Pathology, College of Veterinary Medicine, University of Georgia, Athens, GA 30602, USA

⁸Lead Contact

*Correspondence: mariano.sanchez-lockhart.ctr@mail.mil (M.S.-L.), jit8@cdc.gov (J.S.T.)

<https://doi.org/10.1016/j.cub.2020.10.015>

SUMMARY

Marburg virus (MARV) is among the most virulent pathogens of primates, including humans. Contributors to severe MARV disease include immune response suppression and inflammatory gene dysregulation (“cytokine storm”), leading to systemic damage and often death. Conversely, MARV causes little to no clinical disease in its reservoir host, the Egyptian rousette bat (ERB). Previous genomic and *in vitro* data suggest that a tolerant ERB immune response may underlie MARV avirulence, but no significant examination of this response *in vivo* yet exists. Here, using colony-bred ERBs inoculated with a bat isolate of MARV, we use species-specific antibodies and an immune gene probe array (NanoString) to temporally characterize the transcriptional host response at sites of MARV replication relevant to primate pathogenesis and immunity, including CD14⁺ monocytes/macrophages, critical immune response mediators, primary MARV targets, and skin at the inoculation site, where highest viral loads and initial engagement of antiviral defenses are expected. Our analysis shows that ERBs upregulate canonical antiviral genes typical of mammalian systems, such as *ISG15*, *IFIT1*, and *OAS3*, yet demonstrate a remarkable lack of significant induction of proinflammatory genes classically implicated in primate filoviral pathogenesis, including *CCL8*, *FAS*, and *IL6*. Together, these findings offer the first *in vivo* functional evidence for disease tolerance as an immunological mechanism by which the bat reservoir asymptotically hosts MARV. More broadly, these data highlight factors determining disparate outcomes between reservoir and spillover hosts and defensive strategies likely utilized by bat hosts of other emerging pathogens, knowledge that may guide development of effective antiviral therapies.

INTRODUCTION

Egyptian rousette bats (ERBs, *Rousettus aegyptiacus*), cave-dwelling fruit bats common across sub-Saharan Africa and parts of the Middle East, have been identified as the Marburg virus (MARV) natural reservoir.^{1,2} MARV, a member of the family *Filoviridae* that includes Ebola virus (EBOV), is the only human-pathogenic filovirus for which a natural reservoir has been identified.¹ Filoviruses often cause fatal illness in spillover hosts such as humans and non-human primates (NHPs), yet distinctive of a reservoir species, MARV-infected ERBs remain asymptomatic.^{3–6} Experimentally infected ERBs develop low-level viremia that peaks between days 5–7 post-infection, and typically shed infectious virus in oral secretions for up to 3 weeks.^{3,5,6} Virus disseminates widely, with highest levels found in liver and spleen, before

clearance within ~14 days.^{3,5,6} In contrast, MARV loads in blood of infected NHPs are comparatively high, with death usually occurring within 6–9 days.^{4,7,8} Much remains unknown about how ERBs, along with bat reservoir species harboring other zoonotic pathogens such as Nipah, Hendra, and SARS-related coronaviruses, are able to control viral replication and mitigate the severe disease these agents cause in primates.^{9–11} Elucidating the immunological mechanisms likely facilitating this control in these bats, including cell, pathway, and molecular factors contributing to disease protection, which in turn could inform spillover dynamics and antiviral drug design, has increasingly earned recognition as a core component of global initiatives to prevent and prepare for emerging zoonotic disease outbreaks.

To date, at least two prominent immunoprotective mechanisms in bat reservoirs have been posited. One mechanism,



resistance, suggests that bats are better equipped to control viral replication through noncanonical means, such as quickly mounting innate and adaptive immune responses from a pre-existing high basal state.^{12–14} This strategy has been postulated for large *Pteropus* bats that carry Nipah and Hendra viruses.^{12,13} Another mechanism, disease tolerance, contends that bat hosts have co-evolved with their respective resident pathogens to tolerate infection, allowing viral replication only to levels sufficient enough for transmission while concurrently mounting a subdued antiviral immune response that controls clinical disease (and tissue damage) by actively minimizing proinflammatory responses.^{11,14–17} This concept of tolerance is supported for ERBs, as recent efforts to map the bat's genome and transcriptome has shown that this MARV reservoir (1) has diversified immune-inhibitory domain-containing natural killer (NK) receptor loci and accompanying expansion of major histocompatibility (MHC) loci; (2) has expanded type I interferon (IFN) gene loci, particularly of the IFN ω family, that are less potently induced *in vitro*, suggesting more subdued effector signaling; and (3) fails to induce IFN genes even after ERB cell infection with a mutant MARV that is incapable of antagonizing IFN-stimulated gene (ISG) signaling.^{18–20} Further, infecting ERB bone marrow-derived dendritic cells (BMDCs) failed to increase inflammatory gene expression, while experimental MARV infections of ERBs produced minimal, if any, gross histological signs of inflammation, even in tissues with highest viral loads.^{3,5,6,21,22} The culmination of these data led us to hypothesize that ERBs have indeed developed a system of disease tolerance to MARV. However, significant testing of this hypothesis has so far been limited to immortalized cell lines, *ex vivo* tissue culture infections, or genomic approaches that cannot reproduce or examine the complexity and context of an immune response in a whole animal, which to our knowledge remains uncharacterized at a broad transcriptional level for any bat reservoir of a human-pathogenic virus, including ERBs infected with MARV. A particularly important focus of any *in vivo* host response study in MARV-infected ERBs would be the role of monocytes and macrophages, as these CD14⁺ immune cells, along with dendritic cells (DCs), are primary sites of MARV infection in primates and are critical for initiating innate and adaptive responses.^{4,7,23–25}

To address these critical knowledge gaps, we conduct a 40-animal *in vivo* time course experiment in which ERBs are inoculated with a bat isolate of MARV (or sham control) and euthanized in groups of five on days (D)1, 2, 3, 5, 8, 14, and 28 (or D13 for uninfected control bats).²⁶ All bats come from our captive breeding colony originally founded from ERBs caught in Uganda where ERB-linked MARV outbreaks had occurred. Focusing on early and acute phases of infection, we measure the ERB transcriptional immune response at various tissue sites that are both supportive of MARV replication in ERBs and important in primate filoviral pathogenesis/immunity. These sites include skin at the inoculation site (where viral loads are highest and frontline host defenses are likely) and spleen-derived CD14⁺ monocytes/macrophages, as well as whole spleen, liver, and colon.^{3,6,7,22,24,25} Our study incorporated custom ERB-specific reagents, including an anti-CD14 antibody used in tandem with positive magnetic bead selection (MACS) of CD14⁺ splenocytes and a panel of 380 immune-related gene probes (nCounter ERB CodeSet) used to quantify differential gene expression (DGE) of total RNA extracted

from tissues/CD14⁺ splenocytes. In this report, we demonstrate *in vivo* that disease tolerance is a major strategy by which the ERB reservoir host controls MARV infection, as opposed to a model of initial resistance conferred by more potent antiviral defenses.¹⁴ Specifically, we show significant induction of a cluster of canonical antiviral genes (including *DDX58 [RIG-I]*, *IFIT1*, *IRF7*, *ISG15*, and *OAS3*) typical of viral infection in mammals, but strikingly, almost no significant changes in expression of traditional markers of adaptive immunity or inflammation, including the cytokines and chemokines *IFN γ* , *CCL8*, *FAS*, and *IL6*, normally associated with MARV pathogenesis in primates.^{8,25,27–31} Our findings identify putative virulence-determining differences between reservoir and spillover host, as well as immunoprotective commonalities likely shared between ERBs and bat reservoir hosts of other emerging zoonotic pathogens (e.g., SARS, Ebola), which could be exploitable for human therapeutic development.

RESULTS

CD14⁺ Splenocytes from MARV-Infected ERBs Are Efficiently and Specifically MACS-Selected and Capable of Robust Direct Infection

To validate that our ERB-specific anti-CD14 antibody could be used within our time course MARV infection study to isolate CD14⁺ monocytes/macrophages from ERB spleen with high specificity and efficacy (along with separately using an anti-CD19 antibody to target B lymphocytes), we quantified representative monocyte and lymphocyte populations pre- and post-MACS selection by flow cytometry using total splenocyte suspensions harvested from MARV-infected ERBs during the acute phase of infection at D5. Approximately 12% of splenocytes were CD14⁺, while ~44% stained CD19⁺ (Figures 1A and 1B). These percentages were moderately higher than ranges previously identified for splenic monocytes/macrophages and B cells of other mammals, including NHPs and *P. alecto*.^{32–35} This could be due to infiltration of activated macrophages into the tissue (as the ERB spleens used for cytometry were collected at the peak of viral infection whereas the prior mammalian data were obtained from naive animals), naturally higher basal proportions of resident CD14⁺ splenocytes in ERBs, or some degree of both. Rat immunoglobulin G (IgG) isotype control showed minimal events due to nonspecific protein binding (Figure 1C). These stains were exclusive and based on gating of live, singlet cells (Figure 1C). CD19⁺ cells had a forward-/side-scatter (FSC/SSC) profile indicative of lymphocytes (Figure 1D, red), while CD14⁺ cells were larger and had a profile indicative of monocytes/macrophages (Figure 1D, blue). Following MACS, CD14⁺ and CD19⁺ splenocytes retained both their fluorescence properties (Figures 1E and 1F), with ~95% CD14⁺ enrichment and ~97% CD19⁺ enrichment compared to pre-cell isolation staining or isotype control. Separately, *ex vivo* microscopy of MACS-selected splenocytes from naive colony ERBs also showed morphologies consistent with monocytes/macrophages (CD14⁺) or lymphocytes (CD19⁺), and both populations were homogeneous, in contrast to the heterogeneity of total splenocytes (Figure S1A). To further validate that *in vivo* CD14⁺ splenocyte responses to MARV reflected direct infection of and replication in monocytes/macrophages, which are primary MARV targets in primates, we infected *ex vivo* CD14⁺ splenocytes from naive

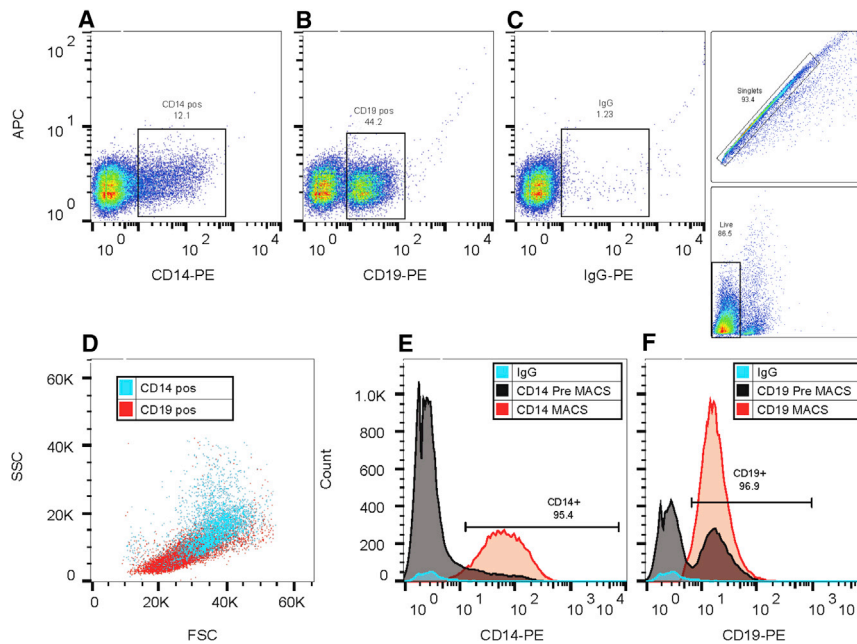


Figure 1. ERB-Specific CD14 and CD19 Antibodies Detect and Magnetically Select CD14⁺ or CD19⁺ Splenocyte Populations with High Efficiency

(A and B) Proportions of live, singlet events for CD14⁺ (A) (consistent with monocytes/macrophages) or CD19⁺ (B) (consistent with B lymphocytes), respectively, as measured by representative PE fluorescence in total splenocyte suspensions harvested from MARV-infected ERBs at D5.

(C) Gating strategy for flow cytometry on singlet, live splenocyte sample events using rat IgG as a negative isotype control stain to differentiate nonspecific antibody binding.

(D) Overlapping forward- and side-scatter (FSC/SSC) profiles of CD14⁺ (blue)/CD19⁺ (red) events as determined in (A and B).

(E and F) Histogram profiles showing post-magnetic bead selection (MACS) enrichment of CD14⁺ or CD19⁺ populations visualized by PE fluorescence (orange), as compared to pre-selected events (determined in A and B, shown in gray) and IgG control events (blue).

See also Figure S1.

colony ERBs with a recombinant version of the same MARV bat isolate used for our ERB inoculations.^{7,21,25,26,36,37} This rMARV encodes a ZsGreen (ZsG) fluorescent protein able to visualize successful filovirus replication.^{36,37} As expected, CD14⁺ populations showed robust *ex vivo* infection, with ZsG fluorescence increasing across the cell monolayer in both breadth and intensity out to D3 (Figure S1B). Thus, these two species-specific antibodies efficiently and selectively target and magnetically isolate ERB cells characteristic of monocytes/macrophages and B cells, agreeing with their cytometric analysis in our previously published BMDC *ex vivo* study, and ERB CD14⁺ monocytic cells are a direct cellular target of MARV infection, reflecting the established MARV tropism of their primate counterparts.^{7,21,25}

MARV-Infected ERBs Become Temporarily Viremic with Virus Dissemination to Tissues

MARV RNA levels in blood were first detected on D1, peaked at D5, and were undetectable by D14 (Figure 2A). Consistent with previous studies, similar viral RNA (vRNA) kinetics were observed in skin at the inoculation site (Figure 2B) and in whole liver and spleen (Figure 2C), persisting in the spleen for longer (D14) than in liver or skin (D8).^{3,6,22} Bat #861 (D5 cohort) had the highest overall vRNA levels detected for any animal and among the highest blood vRNA levels at D4–D5 along with bats #319 (D8), #371 (D28), and #857 (D28), as well as #206 (D14) at D10 (Figures 2A and 2C; Data S1). Characteristic of a negative-sense RNA virus, viral gene counts in skin, as measured by nCounter (Figure 2B, left), showed a mild 3' to 5' transcriptional gradient, while three genomic vRNA targets measuring replication (vRNA 1–3) did not (Figure 2B, right).³⁷ This gradient is also observable in isolated CD14⁺ splenocytes of bat #861 (Figure 2D, left, compared to vRNA targets, right), further indicative of transcription/replication in monocytic cells as previously observed in primate CD14⁺ populations.^{24,25,37} Consistent with data from prior studies of ERBs naturally or experimentally infected with MARV (including histology), and in contrast to reports on severely ill MARV-infected

NHPs, we observed that all infected bats were asymptomatic and tissues were without gross signs of inflammation.^{3,7,22}

Early/Acute Phase Host Gene Responses in MARV-Infected ERB Tissues Indicate Declining Lymphocyte and Increasing Macrophage Proportions

Using total RNA probed with the ERB CodeSet, we analyzed ERB immune response gene expression focusing on CD14⁺ splenocytes and skin (inoculation site). This targeted transcriptomics data allowed us to utilize the CIBERSORT gene expression profiling software to estimate proportionate trends in immune cell populations in skin (Figures 3A and S2A) and spleen (Figures 3B and S2B) over the course of MARV infection. Both tissues consisted of DC, monocyte, macrophage, NK cell, and T and B lymphocyte populations. As expected for mammals, higher estimated proportions of monocytes/macrophages were seen in skin and higher DC and lymphocyte proportions in spleen. NK cells were a small, mostly stable population in both tissues, rising transiently at D5 in spleen during peak viremia but significantly decreasing by D5 and D8 in skin. In skin, mast cells and neutrophils proportionately increased (D1–D5) and decreased (D1–D14) compared to control bats, respectively, with significant proportional neutrophil decline on D8. Consistent with primate studies, B cells showed marked proportional declines by D1 (skin, significantly so from D2–D14) and D5 (spleen) before partially or fully recovering (or even significantly increasing compared to uninfected bats as with splenic B cells from D8–D28).^{4,7} T cell proportions modestly declined in skin (to a significant degree on D8) without fully recovering by D28. Conversely, macrophage proportions increased (D2–D5) in skin and spleen, the latter of which show significant increases on D2 and D5, coincidentally with a proportional reduction of monocytes between those time points. However, monocyte proportions in skin overall showed expansion across the time course (significantly on D8 and D14) compared to uninfected bats; based on population trends for individual bats (Figure S2A), this expansion appears

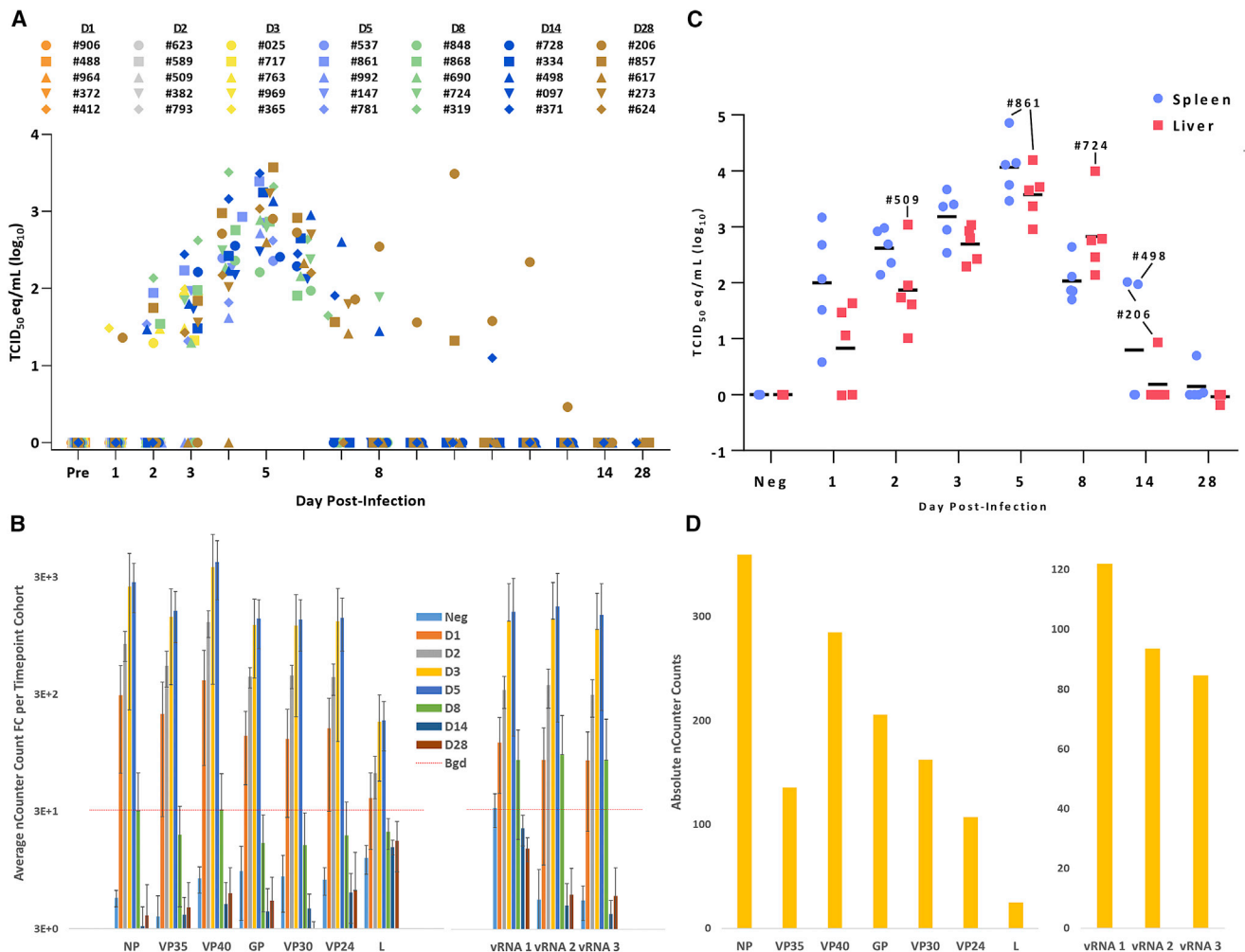


Figure 2. Viral RNA Is Detected in Blood, Skin, and Whole Tissues from MARV-Infected ERBs with Kinetics like Previous Studies and Indicates Viral Gene Transcription and Replication in CD14⁺ Splenocytes

(A) Daily viral RNA levels of all remaining individual bats were quantitated by MARV TaqMan assay of total RNA extracted from whole blood. Each time point cohort was color-coded as indicated in figure legend at top, with each bat denoted by a different symbol. Pre, pre-inoculation.

(B) RNA level in skin for each nCounter-based MARV gene (left side) or each of three vRNA targets (right side) following nSolver analysis was calculated using the average normalized counts for each infected or control bat cohort. Error bars indicate standard deviation of the averaged counts. Dotted red lines indicate background count threshold value.

(C) Viral RNA levels for each individual bat were quantitated by MARV TaqMan assay of total RNA extracted from liver and spleen.

(D) CD14⁺ splenocyte nCounter-based normalized viral gene counts (left) or vRNA counts (right) were calculated for bat #861, the only bat in the CD14⁺ dataset with MARV targets above background.

to only lack statistical significance prior to D8 due to an unusually high monocyte percentage identified for bat #557 among uninfected cohort members. Finally, bat #861 (D5), which had the highest splenic viral load, showed the greatest reduction in B cell percentage and greatest increase of NK/macrophage proportions of all bats for that tissue type (Figure S2B).

MARV-Infected ERBs Show Broad Gene Induction in CD14⁺ Splenocytes and Skin but an Overall Moderate, Transient Immune Response that Includes Genes from Functionally Related Classes

We measured fold-change (FC) of significantly differentially expressed genes (DEGs) in RNA from CD14⁺ splenocytes, skin,

and whole tissues (spleen, liver, and colon/rectum) of MARV-infected ERBs using the nCounter Advanced Analysis (nCAA) software module. Both CD14⁺ splenocytes and skin showed early gene induction (D1) and had highest DEG numbers (Figure S2C). Skin and CD14⁺ splenocytes had 36 and 63 unique DEGs, respectively, and shared an additional 42 targets (Figure S2D; Table S1). Many of these unique and shared DEGs were from functionally related gene classes. Complement and apoptosis factors, IFN type I/II-related genes, and lymphocyte/DC/macrophage markers and regulatory genes were notable DEG classes unique to skin (Table S1). CD14⁺ splenocyte-specific DEGs included viral restriction, cell growth/stress response, and anti-inflammatory factors, as well as TNF and kinase family members

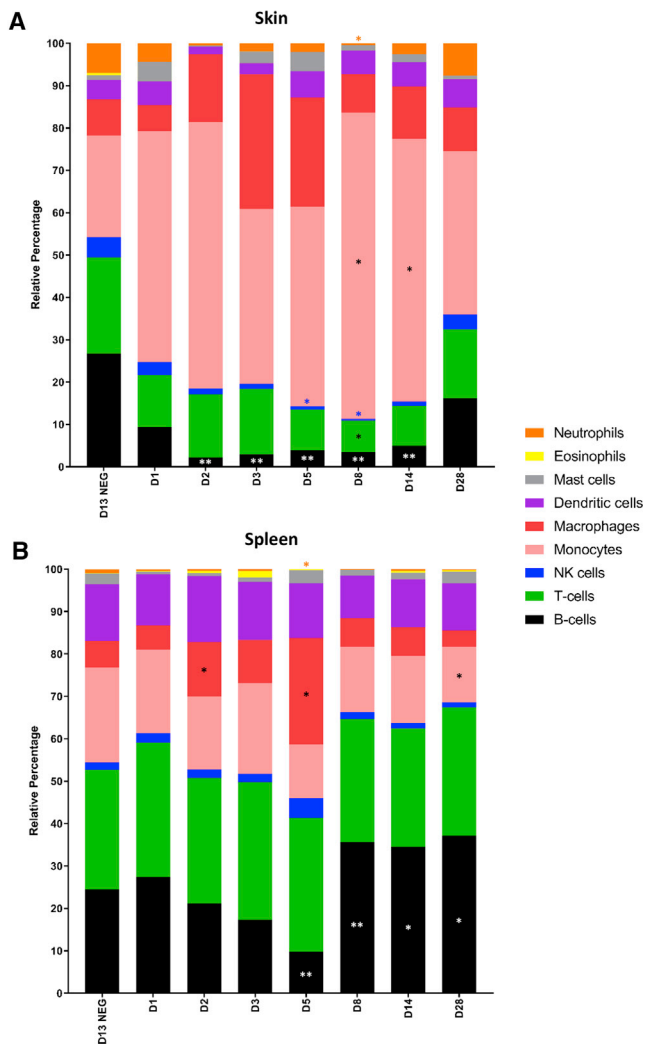


Figure 3. Skin and Spleen Gene Expression Patterns Suggest Lymphocyte Depletion and Monocyte Expansion following MARV Infection of ERBs

Normalized nCounter gene counts from tissue datasets were analyzed by the web-based CIBERSORT program to match time point-averaged ERB gene expression from (A) skin or (B) spleen, to known signatures identified for human marker genes of various immune cell types. Immune cell types identified in each tissue are represented by color, and bar length of each indicates the relative estimated percentage of that cell type present within the total mixed-cell population. Black and white asterisks denote significant p values ≤ 0.05 (*) or 0.01 (**) obtained by two-tailed t test for individual cell types in each infected bat tissue in comparison to their estimated proportions in uninfected control bats; colored asterisks correspond to the identically colored cell type below them. See also Figure S2.

(Table S1). Skin and CD14⁺ splenocytes shared interleukin (IL)-related genes and IFN regulatory factors (IRFs), which were mostly induced in CD14⁺ splenocytes, whereas almost all co-stimulator upregulation occurred in skin. Colon and liver shared some viral entry, replication/DNA damage response, and egress-related antiviral DEGs with skin, including *SAMD9L*, poly (ADP-ribose) polymerases (*PARPs*) and *PML*, and *BST2* (*Tetherin*), respectively (Table S1). Further, skin and/or CD14⁺ splenocytes shared induction of MHC-related factors, including

beta 2-microglobulin (*B2M*) and *HLAs* with liver (Table S1), which may be linked to the recently identified expansion of MHC class I genes within the ERB genome.¹⁸ Lastly, limited sets of DEGs were unique to and shared among other tissue/cell groupings, including one DEG each specific to liver (*TIGIT*), colon (*HSH2D*), and spleen (*CD163*) (Figure S2D; Table S1).

Globally averaged FC levels across datasets were modest: less than 16-fold in skin (where viral load was highest) and barely extending beyond ~7-fold in CD14⁺ splenocytes (Figure S2C). Primary responses were also temporally limited, usually peaking by D2 (CD14⁺ splenocytes and whole tissues) or D3 (skin) and quickly returning to baseline by D5–D8 (CD14⁺ splenocytes and tissues) or by D8–D14 (skin) (Figure S2C). Peak responses occurred within the early exponential phase of viral replication, just prior to maximal viral loads (compare Figure S2C to Figure 2). Significant downregulation, an otherwise rare occurrence seen at select time points for few DEGs, was observed in spleen at D8 (Figure S2C).

The Transcriptional Immune Response to MARV in ERBs Is Characterized by Early and Acute-Phase Induction of Canonical Antiviral Genes and Pathways Typical of Mammalian Systems

To better visualize immune response progression in MARV-infected ERBs, we generated heatmaps of nCAA-derived, time point-averaged DEG datasets (Figures 4 and 5). In addition to our core analysis of CD14⁺ splenocytes, skin, and whole tissues (spleen, liver, and colon) in which viral replication has been previously observed, we separately analyzed antiviral gene expression in CD19⁺ splenocytes (Figure S3).^{3,6} As this expression profile was largely similar to that found for CD14⁺ splenocytes, and was presumably indirect as B lymphocytes are not a known MARV replication target in any species, we excluded this dataset from comparative analyses in this study.⁴ Among the five core tissue/cell types, we further discriminated potential trends by categorizing DEGs into various generalized response networks with functional roles annotated by PANTHER and DAVID programs (denoted by color-coded squares in Figures 4 and 5). The clearest response trend was a common cluster of 26 DEGs (D2–D5) that accounted for the most strongly upregulated genes (denoted by asterisks in Figures 4 and 5); 14 DEGs within the cluster were shared by four of these tissue/cell types, while the other 12 were upregulated in all five types. The cluster was dominated by canonical antiviral factors usually upregulated in mammalian immune responses and involved in IFN induction (*IRF7*, *IFI6*, *XAF1*) and/or antiviral defenses such as pattern recognition (*DDX58* [*RIG-I*], *EIF2AK2* [*PKR*]), ISGylation (*ISG15*, *HERC5*, *USP18*), the RNase L pathway (*OAS3*), and ISG effector functioning (*MX1*, *IFIT1/2*, *STAT1*).^{25,28,29,31,38} Some were significantly but transiently downregulated in spleen on D8 (*CD163*, *RIG-I*, *ISG15*, *USP18*), most after strong initial induction (Figure 5C). Indeed, all but one of the three highest-induced genes across tissue/cell types were cluster DEGs, except late (D14) upregulation of *IL8* in skin, which was the study's strongest induced gene. A hierarchy of induction was also noted within the cluster, particularly *ISG15*, the leading DEG in liver and colon, among the top three in spleen and CD14⁺ splenocytes, and followed by *COMP*, *OAS1*, *IFI6*, and *DHX58* (Figures 4 and 5). These

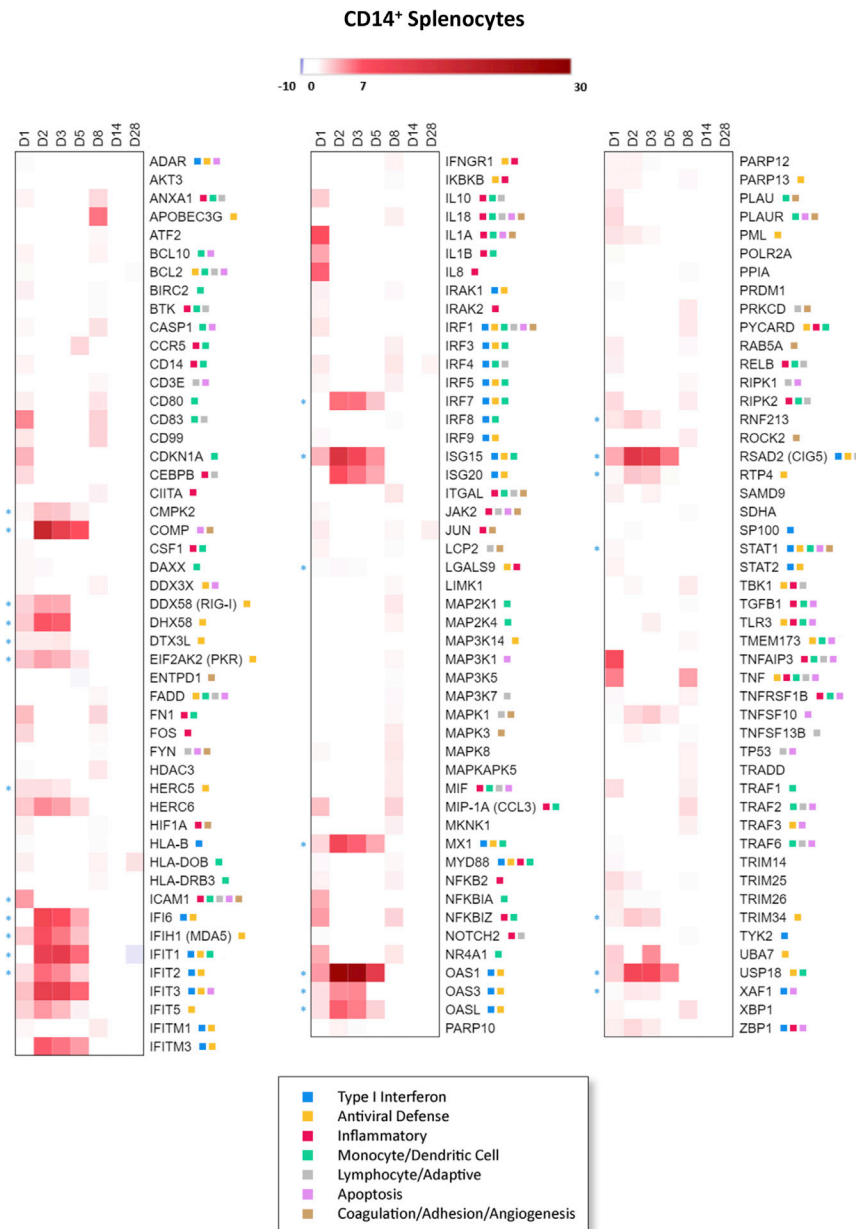


Figure 4. The ERB Transcriptional Immune Response to MARV Infection in CD14⁺ Splenocytes

nCAA analyzed differential gene expression (DGE) using gene counts of infected versus uninfected bats for CD14⁺ splenocytes. Selection as a differentially expressed gene (DEG) at each time point was based on meeting ± 2 fold-change (FC), p value ≤ 0.05 , and above-background count criteria (described in Methods). At a minimum, DEGs met these criteria at one or more time points in each dataset. A heatmap was produced using Morpheus. Linear FC intensity for each DEG was denoted in red (upregulation), blue (downregulation), or white (no change/failed criteria). Only datapoints meeting above inclusion criteria were visualized. Each column denotes a different time point, as indicated on top of each graph. Gradient bars represent FC intensity scales, set to a maximum of 30-fold. Blue asterisks denote the cluster of 26 canonical antiviral genes common to at least four of the five major datasets. Color-coded squares next to most DEGs denote their functional annotation by PANTHER and DAVID programs within generalized response networks as indicated in the bottom legend.

See also Figures S2, S3, and S4 and Tables S1, S2, S3, and S4.

bat #861 (D5), which generally had the highest viral loads and showed markedly greater global induction of DEGs than other bats within its time point cohort in CD14⁺ splenocytes or whole tissues. Collectively, DEG profiles between nCounter analysis methods (nCAA-derived versus individually quantitated) were similar.

Finally, to discern in which main signaling pathways the DEGs sets may be involved, we performed Ingenuity Pathway Analysis (IPA). Two pathways were unique to CD14⁺ splenocytes: “Toll-like Receptor (TLR) Signaling” and “[DC] Maturation,” the latter of which is expected for a monocyte-enriched population (Figure 6A). IPA of skin featured

five genes alone accounted for 11 of the 15 top three DEGs across the five tissue/cell types. Despite strong upregulation relative to other ERB DEGs, cluster gene induction showed markedly reduced potency when compared qualitatively to previously reported gene induction for NHP homologs in whole blood, total peripheral blood mononuclear cells (PBMCs), or PBMC-derived immune cells (including CD14⁺ monocytes) following *in vivo* infection with various MARV or EBOV isolates.^{25,28,29,31,39}

Complementary heatmaps based on the DEGs identified by nCAA, inclusive of each infected bat, were also produced (Figures S4 and S5). Immune response profiles of individual bats within a cohort were generally very consistent. Further, this analysis revealed broad response intensity differences for individual bats that correlated with their vRNA levels. The clearest example was

entirely unique positively regulated pathways: “JAK/STAT Signaling,” “IL6 Signaling,” “IL10 Signaling,” “Th2 Pathway,” and “Role of Macrophages, Fibroblasts and Endothelial Cells in Rheumatoid Arthritis,” potentially selected due to infiltration of immune cells into the inoculation site (Figure 6B). Strong positive regulation of IL6, JAK/STAT, and Th2 pathways extended to D28, perhaps because of virus lingering within the site. CD14⁺ splenocytes shared two innate immune response pathways with whole tissues (Figures 6C–6E): “Activation of IRF by Cytosolic Pattern Recognition Receptors [PRRs]” and “Role of [PRRs] in Recognition of Bacteria and Viruses.” Two other immune response pathways were unique to all whole tissues: IFN signaling and “Role of RIG-I Receptors in Antiviral Innate Immunity.” Most immune response-related pathways showed strong positive regulation, particularly during early/acute phases (D2–D5).

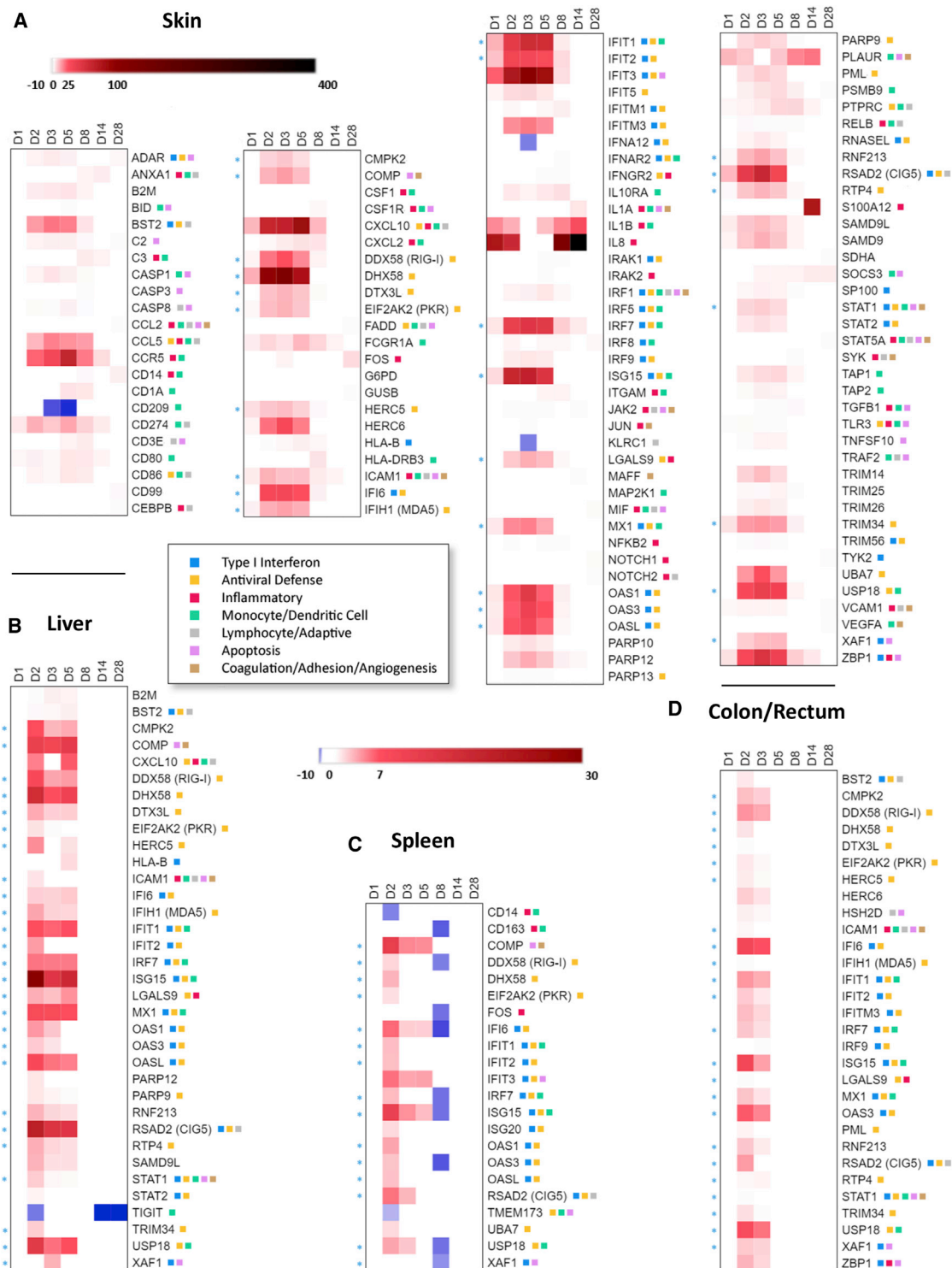


Figure 5. The ERB Transcriptional Immune Response to MARV Infection in Skin and Whole Tissues

nCAA analyzed DGE as described in Figure 4 for each tissue dataset: (A) skin/inoculation site (across top), (B) liver, (C) spleen, (D) colon. Heatmaps were produced as described in Figure 4. Gradient bars represent FC intensity scales, set to a maximum of 30-fold and identical for all datasets except skin (bar at top), which instead has a maximum of 400-fold. Blue asterisks denote the cluster of 26 canonical antiviral genes common to at least four of the five major datasets. Color-coded squares next to most DEGs denote their functional annotation by PANTHER and DAVID programs within generalized response networks as indicated in the center legend.

See also Figures S2 and S5 and Tables S1, S2, S3, and S4.

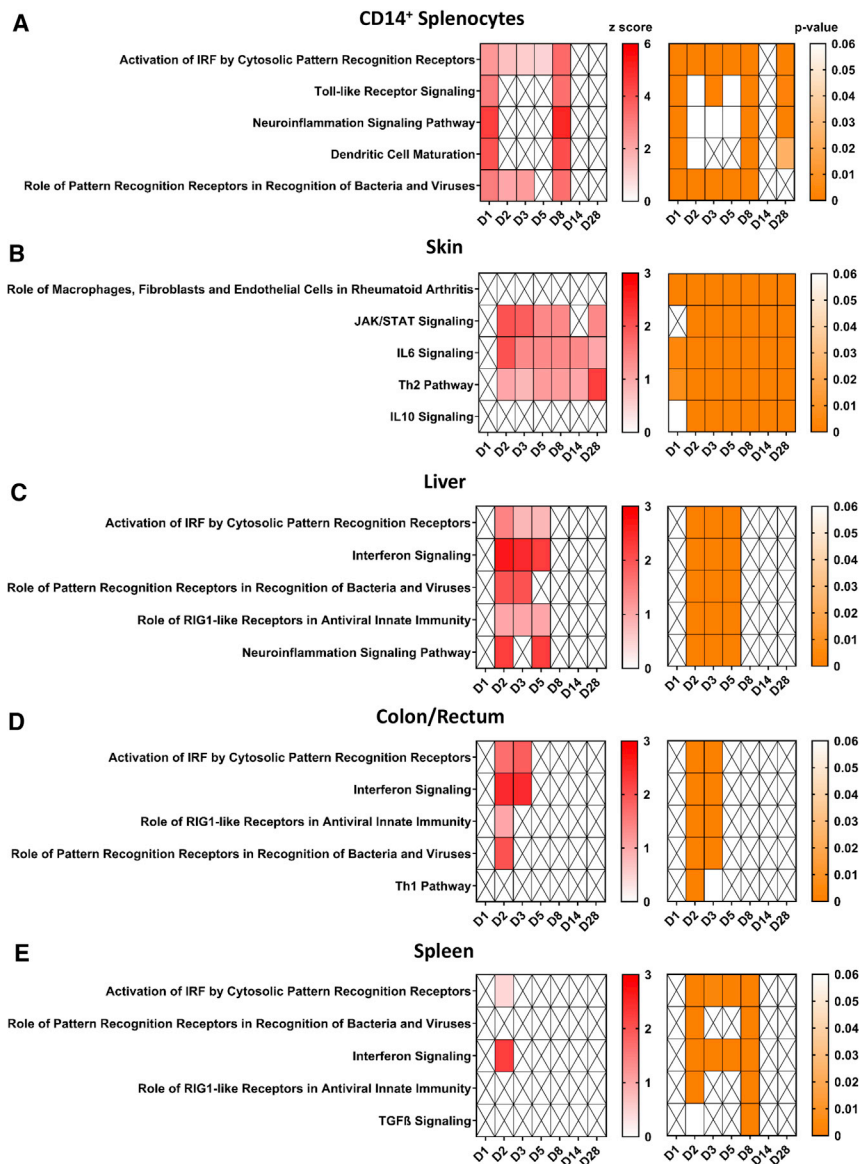


Figure 6. A Handful of Canonical Signaling Pathways Regulated in CD14⁺ Splenocytes, Skin, and Whole Tissues Define ERB Transcriptional Immune Responses

Ingenuity pathway analysis (IPA) was used to determine the top five canonical pathways for each major dataset: (A) CD14⁺ splenocytes, (B) skin/inoculation site, (C) liver, (D) colon, and (E) spleen. Top five pathways are ranked by p value. Z score specifies an activation score calculated by IPA where a positive value indicates that the gene expression in the dataset is changing in a way that suggests positive regulation. Negative values indicate that the gene expression in the dataset is changing in a way that suggests negative regulation. Pathways without a calculated Z score are indicated with an “x.”

adaptive immune response-related gene markers or receptors, including *CD19*, *CD8A/B*, *FOXP3*, *HLA-A*, *HAVCR1/2*, and *KLRs*, were also unaltered (Tables S2 and S3).

Notably, we observed that many pro- and anti-inflammatory and receptor genes, including cytokines, chemokines, and adaptive immunity-related genes, were not significantly induced in MARV-infected ERBs (Table S4). Among them were most IFN genes, *CXCL11*, *CCL8*, *CSF2* (*GM-CSF*); various IL genes such as *IL6*, *IL33*, *GZMA*, and *NOS2/3*; and receptors including *CD40*, *FAS*, *IFNAR1*, and *IL6R*.

To further clarify the impact of the minimally regulated cytokine and chemokine signaling/receptor pathway in CD14⁺ splenocytes and skin of infected ERBs, we used Pathview Web to visualize regulation of over 80 DEG and non-DEG pathway members present in the ERB CodeSet. The lack of significant cytokine, chemokine, or receptor induction identified

ERB Response to MARV Shows Minimal Regulation of Cytokine, Chemokine, and Adaptive Immunity-Related Genes

While ERB immune-related gene induction reflected typical mammalian responses (albeit with reduced potency than observed in filovirus-infected NHPs), we wanted to determine if any DEGs previously identified in MARV-infected spillover hosts (like NHPs) were not significantly regulated in the natural bat reservoir.^{25,38,39} Thus, we compiled all genes within our ERB CodeSet not defined by nCAA as significant DEGs (Tables S2, S3, and S4); these were nearly half the CodeSet’s genes. Many non-DEGs were signaling intermediates or transcription factors (Table S2), including those not usually upregulated such as *MAVS*, *JAKs*, *STATs*, *CTNBN1*, MAP kinase genes, and *MYC*. Other genes unchanged following MARV infection of ERBs have known involvement in antiviral responses, including *DDX50*, *IFI35*, *MX2*, *OAS2*, and *UBE2L6*. Several innate and/or

identified by Pathview was remarkable. In CD14⁺ splenocytes, cytokine induction was mostly limited to the overall modest D1 response, with strongest but transient induction of *IL8*, *IL1A/B*, and *TNF* (Figure 7). In skin at the inoculation site, where presence of these inflammatory response factors is expected due to the high viral load at this location following MARV inoculation, only a handful were identified as significantly upregulated, particularly *IL8*, *IL1B*, *CXCL10* (*IP10*), *CCL5* (*RANTES*), and *CCR5* (Figure S6A). Few additional genes with any role in inflammation as annotated by PANTHER and DAVID programs were induced beyond low, often transient levels, including *TNFAIP3* (CD14⁺), *ICAM1*, and *LGALS9* (CD14⁺ and skin) and *CXCL2*, *S100A12*, and *ZBP1* (skin) (Figures 4 and 5). Overall, inflammatory responses contrasted with those for other antiviral pathways such as RIG-I, TLR, and TNF signaling, which showed significant DEG involvement in skin and CD14⁺ splenocyte datasets during early/acute phases of MARV infection (Figures S6 and S7).

CD14⁺ Splenocytes

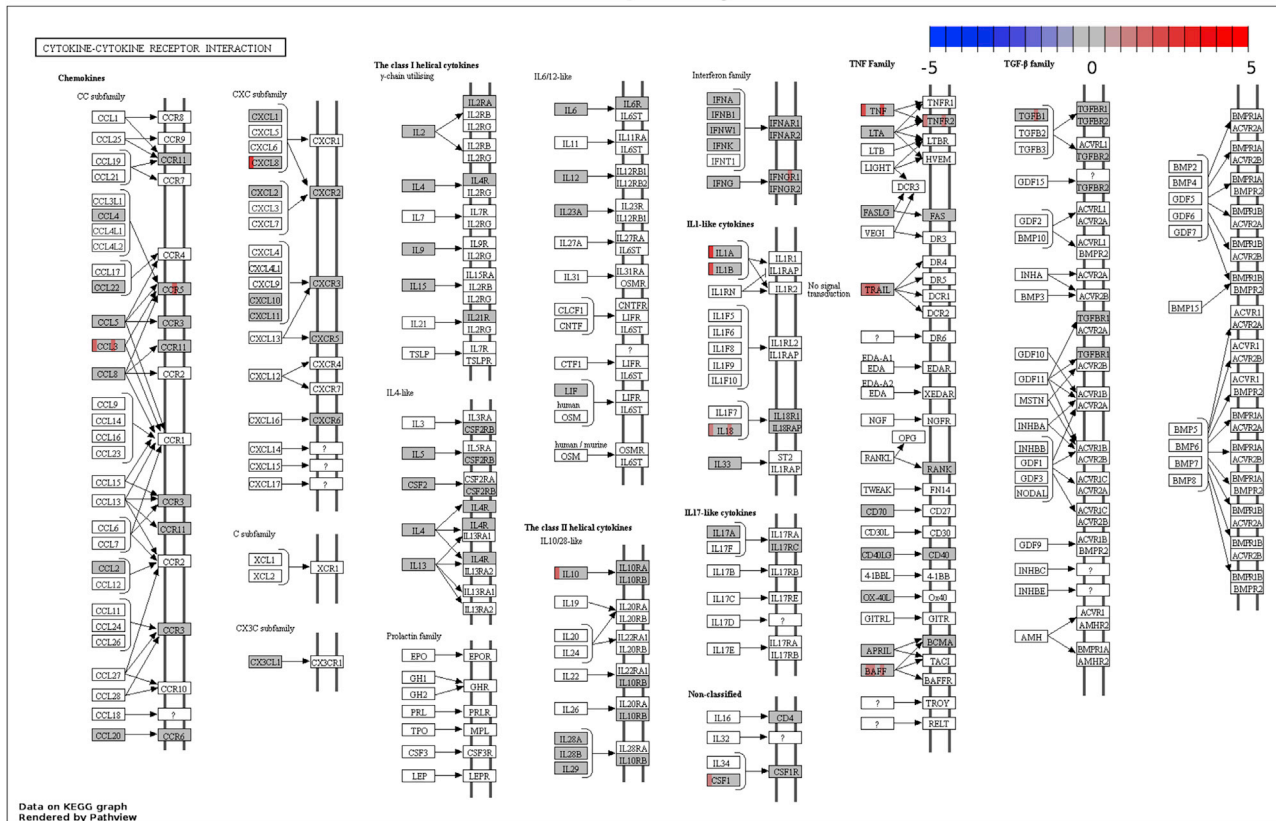


Figure 7. ERB Transcriptional Immune Responses Occur in the Absence of Significant Expression Changes for All but a Few Cytokine and Chemokine Signaling/Receptor Genes

Pathview Web analysis shows representative DGE of the cytokine/chemokine receptor interaction pathway for CD14⁺ splenocytes. Genes in white boxes are those without ERB CodeSet probes; genes in greyed boxes are those represented in the CodeSet. Red bands indicate upregulation of a given gene, blue bands indicate downregulation, and gray bands indicate lack of expression change/failed inclusion criteria; each band indicates a different post-infection time point from D1 to D28, arranged left to right across a gene box. Legend at top right defines color intensity scale set at indicated log₂FC values.

See also [Figures S6 and S7](#) and [Table S4](#).

DISCUSSION

Soon after the discovery of MARV, key questions quickly emerged, including what the natural reservoir is, how the virus spills over into humans and NHPs, and importantly, how does the reservoir host immunologically control the pathogen while allowing sufficient viral replication to enable transmission.^{1,2,5,6,11,15} In this report, we characterize the *in vivo* transcriptional immune response in MARV natural reservoir, focusing on CD14⁺ splenocytes and skin at the inoculation site, both pathogenesis-relevant sites of virus replication.

DGE analysis across tissue datasets revealed a broad, distinctive host response in which inflammatory genes and their receptors were not significantly changed in MARV-infected ERBs, in stark contrast to the extensive dysregulation seen in primates.^{7,27–29,31,39} While we cannot completely rule out non-canonical strategies by which some non-DEGs could contribute to MARV resistance (e.g., enhanced basal expression that “primes” ERBs to better engage antiviral defenses, as demonstrated in *Pteropus* bats), this transcriptional phenotype offers the first *in vivo* functional evidence for disease tolerance in a

filovirus reservoir.^{11,12,14–16} In this scenario, the antiviral state in MARV-infected ERBs would restrict replication while avoiding immune-mediated pathology caused by cytokine and chemokine dysregulation. Thus, the absence of DEGs thought to cause such pathology is remarkable and holds at least three major implications regarding the differences in pathogenesis between infected reservoirs and accidental spillover hosts and the exact physiological avenues by which reservoirs and viruses co-evolved a tolerant host environment. First, the paucity of significant cytokine/chemokine responses in ERBs is clearly distinct from those observed in filovirus-infected primates and relates to disease burden.^{7,8,27,28,30,31} Only a handful of such genes (including *CCL5*, *IP10*, *IL1B*, *IL8*, and *TNF*) were significantly up-regulated either at the infection site or transiently in CD14⁺ splenocytes and almost none in whole tissues, consistent with previous clinical observations of minimal tissue inflammation in ERBs.^{3,6} Non-DEG cytokines/chemokines within the ERB CodeSet included most *IFNs*, *ILs* such as *IL12B* and *IL33*, *NOS* genes, and a few *CCLs*, *CCRs*, and *CXCRs*. Indeed, recently published *in vitro* data from our lab using MARV-infected ERB BMDCs also showed limited inflammatory gene regulation, expanding

support for ERB disease tolerance to MARV.²¹ One notable distinction between our current *in vivo*-based work and the BMDC study was that *IL33* was strongly suppressed in BMDCs, which might simply suggest DC-specific gene regulation. Meanwhile, the lack of significant induction of *IFNs* agrees with previous data from an ERB kidney cell line even after being infected with a recombinant MARV ablated in its usual ability to antagonize IFN-mediated antiviral gene induction via VP35, and despite those cells showing marked induction of multiple IFN genes by an unrelated control virus (Sendai virus).¹⁹ Type I IFN genes also showed minimal, if any, detectable basal gene counts in uninfected bats, suggesting that ERBs do not rely on constitutively activated IFN as posited for *P. alecto* bats by Zhou et al.¹² It is tempting to speculate that IFN-independent responses therefore occur in these animals, allowing induction of specific antiviral genes even in the presence of viral antagonist proteins. For instance, recent work by the Mühlberger lab showed that MARV VP35 inhibits PKR in human but not ERB cells, and there is precedent for IFN-independent response induction by IRF3 or STAT1 of subsets of canonical antiviral genes during *in vitro* human cytomegalovirus (HCMV) infection.^{40–42} This does not preclude, however, the alternative possibilities that induction of IFN gene transcription simply occurs at levels too low for nCounter to detect, certain IFN proteins are activated on a post-transcriptional level, and/or the ability of MARV proteins to fully suppress IFN is cell type-dependent, any of which would suggest that IFNs still act as master antiviral response regulators in MARV-infected ERBs, perhaps in a paracrine fashion, without a need for noncanonical explanations. Of most relevance to pathogenesis among the cytokine/chemokine non-DEGs in ERBs is that they appear to be largely pro- or ambi-inflammatory; several are highly induced in primate filoviral infections, including *IFN γ* , *IL2*, *IL4*, *MIP-1 β* (*CCL4*), and *CSF2*.^{8,24,25,27,30,31,39} Indeed, *CCL8*, *FAS*, and particularly *IL6* are commonly reported hallmarks of the primate inflammatory response and subsequent severe disease.^{24,27,39} While basally expressed in naive ERBs, none of these genes displayed any significant activation upon MARV infection, suggesting no role in the ERB response to MARV, again consistent with a disease tolerance model.^{11,14–16} Second, tolerance may offer a molecular explanation for why these bats have previously exhibited non-neutralizing antibody activity when tested *in vitro* and rapidly waning IgG in serum despite protective secondary responses upon MARV rechallenge.⁴³ Our data show insufficient adaptive immune gene induction (such as *AGER*, *CD40*, *HLA-A*, *IL13*, and *TNFSF13*) that could be associated with unique mechanisms dictating lymphocyte maturation, Ig structure/function and/or memory cell generation/activity. Prior genomic studies have posited that in some bat species, there is a diminished emphasis on the role of somatic hypermutation, which could subsequently lessen a role for IgG during primary acute infection and potentially promote dampened antibody-mediated inflammation.¹⁰ Our results extend the possibility of quantitatively reduced adaptive immunity to ERBs on a transcriptional level. We also identified (likely indirect) antiviral gene expression in CD19⁺ splenocytes following MARV infection, possibly affecting the role of B cells in adaptive immune processes, as well as a conspicuous proportional reduction of skin and spleen B cells in our CIBERSORT analysis. This latter data suggest depletion of

lymphocytes from these tissues at around or just prior to when MARV-infected ERBs exhibit initial IgG production, which could possibly further contribute to the IgG response phenotype and/or reduced antibody-mediated inflammation.^{4–6,44} Given these open questions, a better understanding of antibody loci, development, and response in these animals is required. Third, this finding offers insight into the broader spectrum of antiviral response strategies used by viral reservoir hosts *in vivo*, and into how disease tolerance in ERBs compares to other host-virus relationships. This relationship has been well characterized for hantavirus rodent hosts. Like ERBs, bank voles (*Myodes glareolus*), male Norway rats (*Rattus norvegicus*), and deer mice (*Peromyscus maniculatus*) infected with Puumala virus, Seoul virus, or Sin Nombre virus, respectively, show no clinical signs of disease, lack tissue-specific proinflammatory cytokine induction, and generate low or non-neutralizing antibody responses.^{45–48} Disease tolerance has also been suggested in studies with raccoons infected with raccoon rabies virus and mallards infected with low-pathogenic H1N1.^{49,50} However, to our knowledge, no other significant *in vivo* study of broad transcriptional immune responses in any bona fide bat reservoir has been performed. Coronavirus inoculation of a suspected but unconfirmed ancestral reservoir, the Jamaican fruit bat (*Artibeus jamaicensis*), resulted in subclinical disease and transient, low-level induction of *MX1*, *IFIT1*, and *RANTES*, supporting tolerance.⁵¹ More recently, a second, proteomics-based study compared the lungs of Hendra virus-infected *P. alecto* bats and ferrets 60 h post-infection, in conjunction with limited IFN and cytokine TaqMan analysis.⁵² This report found downregulation of constitutively expressed IFN in these bats, with a significantly more likely enhancement of IFN signaling and neutrophil-, T cell-, and antibody-mediated immunity pathways than ferrets, suggesting inflammatory response suppression amidst concomitant cell-mediated response activation. These two studies, however, remain rare examples of *in vivo* immune response data for bats. Intra-order comparisons beyond gross clinical observations thus remain challenging, highlighting the necessity for expanded *in vivo* reservoir host research to capture a more comprehensive and contextual picture of the complex biological processes that follow infection by pertinent pathogenic threats like filoviruses. The overarching immunological principles and precise host factors dictating reservoir protection against disease that such studies uncover have become essential in a globalizing world where human contact with wild hosts, and emerging disease outbreaks from the viruses they harbor, becomes an ever more frequent event, as the likely recent spillover of SARS-CoV-2 from an unidentified bat reservoir has illustrated to a profoundly devastating effect.

DGE analysis also revealed commonalities and differences between significant ERB and primate responses, as well as the potential importance of several specific DEGs. MARV infection of ERBs stimulated canonical immune response genes, such as *ISG15*, *IFIT2*, *RIG-I*, and *OAS1*.^{28,38} Similar upregulation was not seen previously using MARV-infected ERB cell lines; rather, antiviral genes were largely suppressed.¹⁹ The apparent discrepancy in immune gene signaling between infected cells and whole animals has also been reported in primate studies, again emphasizing the value of investigating *in vivo* host responses.²⁴ This phenotypic disagreement between *in vitro* and

in vivo responses may be due in part to conditional roles of aforementioned viral antagonists like VP35, which at high multiplicity of infection common for *in vitro* assays could accentuate suppressive antagonist abilities (another potential explanation for the lack of significant *IL33* induction *in vivo* compared to BMDCs).^{19,21,53} Further, their functions could be restricted temporally or by cell type and/or unresolvable in mixed cell populations. Indeed, primate macrophages, a primary filoviral target, show robust antiviral gene responses both *in vitro* and *in vivo* following EBOV infection, as do the ERB-derived BMDCs after *ex vivo* MARV infection, both reflecting those we observed *in vivo* in MARV-infected ERB CD14⁺ splenocytes.^{21,24,25} Comparing *in vivo* data from our work using the ERB-derived MARV isolate 371Bat2007 to data from filoviral primate studies is vital to understanding how the natural reservoir has evolved to better control infection compared to the maladaptive immunopathology elicited in primate spillover hosts. For instance, most MARV primate experiments use the Musoke or Angola virus isolates that, at the whole-genome level, are ~93% identical to each other and ~92% identical to 371Bat2007. Importantly, each of these viruses is linked to, or isolated from, fatal human infections and causes near-uniformly fatal disease in NHPs. Indeed, the MARV bat isolate used in our study is greater than 99% identical to 01Uga07, a virus isolated from a fatally infected miner working at Kitaka mine in Uganda where the ERB harboring 371Bat2007 was captured.^{26,54} Therefore, the high degree of sequence identity between 371Bat2007 and 01Uga07, combined with the known diversity among fatal human filoviruses, strongly suggests that this bat isolate would also cause severe, if not lethal, disease in primates. To this end, DEGs in MARV-infected ERBs consisted of canonical antiviral genes typical of those seen in infected primates and other mammalian systems.^{25,28,29,31,38} Most, if not all, of the 26 cluster DEGs common across ERB tissues/cells, such as *ISG15*, *OAS1*, and *MX1*, have also been identified as elevated in MARV-infected primates.^{25,29,31} Moreover, cluster DEGs acted within a limited spectrum of traditional pathways shared by primates and other bat species, such as OAS/RNase L signaling, ISGylation, and JAK/STAT signaling.^{13,25,31,53} Assuming these ERB genes have antiviral capabilities akin to their primate orthologs, this implies that cluster gene induction alone does not confer MARV protection to ERBs, as we hypothesized in our ERB kidney cell line-based study.¹⁹ However, these data suggest that antiviral responses are better regulated in ERBs than in primates, with a subset of genes dictating a large proportion of the global response but confined to a short-lived induction window in which these presumably normal responses are actively controlled. Further, ERB response genes were substantially less induced than those previously measured in primate whole blood, monocytes, or tissues.^{25,29,31,39} For a probable ERB infection target like CD14⁺ splenocytes to show mostly as limited, tightly regulated, and canonical a response profile as ERB whole tissues, whereas in primates these immune cells show extensive, strong ISG, and adaptive immune and inflammatory gene responses, is perhaps also indicative of disease tolerance.²⁵ Among non-cluster DEGs, some showed notable changes. The intense mid/late upregulation of *IL8*, *IL1B*, and *S100A12* at the skin inoculation site was possibly due to an uncleared bolus of virus and/or prolonged immune cell infiltration. Conversely, several DEGs downregulated D2–

D3 in skin and spleen play roles in transitional innate-adaptive processes, including T cell activation by DCs (*DC-SIGN*, also a filovirus receptor), NK cell recognition of MHC class I molecules (*KLRC1* [*NKG2*]), T cell activation via MHC class II-presenting B cells (*TMEM173* [*STING*]), and monocyte-macrophage differentiation (*CD14*). Suppressing these factors could impact established downstream features of MARV pathogenesis, such as lymphopenia due to lack of DC maturation and T cell activation (which itself modulates antibody production).^{4,7,8}

Another notable aspect of our study was an ability to correlate MARV replication levels with specific ERB immune response gene kinetics across tissue/cell types, including at early and acute time points post-infection, thereby greatly expanding upon previous work that was able to detect only MARV RNA in these tissues.^{3,6} Indeed, virus disseminated quickly from the inoculation site, evidenced by virus positivity in spleen and liver by D1 and corresponding broad early host gene induction in skin and CD14⁺ splenocytes. This D1 response in CD14⁺ splenocytes occurred prior to responses in the surrounding spleen tissue. These kinetics leave open the likely possibility that infiltrating monocytes may be initially infected at the inoculation site and then transport the virus into the spleen and other tissues. Thus, CD14⁺ splenocyte response induction following infection, replication, and viral protein expression is likely critical to MARV pathogenesis, irrespective of infectious virion formation from this cell type (not specifically measured in the context of this study), which might very well guide toward a non-productive infection given a fully functional, co-evolved ERB immune system capable of mitigating viral disease burden. Further, since B lymphocytes are not known to be MARV replication targets, any observed antiviral gene transcription in CD19⁺ splenocytes is likely due to paracrine induction by host factors secreted from these early infected spleen monocytes.⁴ Indeed, as the majority of total splenocytes (~56%) consisted of CD14⁺ and CD19⁺ cells and expression profiles were largely similar between them, upregulation of their DEGs probably formed the basis of the overall response seen for whole spleen. Despite the early kinetics in skin and CD14⁺ splenocytes, onset of the bulk of the host response was delayed until D2. Responses correlated with viral load through D5. As identified by CIBERSORT in the skin and spleen, kinetics of viral loads and/or immune responses also corresponded to proportional, in some cases significant, estimated changes in lymphocyte and macrophage populations indicative of cell depletion/apoptosis and activation/infiltration, respectively (although we must caveat that this analysis is based solely on gene expression data from our large, though finite, ERB CodeSet and will need validation in future studies in order to rule out possible biases due to reliance on nCounter values or human-specific marker gene signatures). Nevertheless, together these observations suggest that innate immunity in ERBs, capable of robust upregulation even during peak infection, swiftly controls viral replication, possibly without substantial lymphocytic support. Simultaneously, negative feedback pressures (e.g., *USP18*, a known IFN signaling modulator) coordinate equally rapid cessation of primary gene responses once virus control is secured. The correlation of viral replication to host response also implies proportionality in individual bats. For example, as seen in bat #861, high viral load may be linked to transcriptional “superinduction” and immune cell population phenotypes. This putative relationship

raises intriguing questions regarding host susceptibility (whether bats under stressful or immunomodulating conditions permit greater viral replication), immune adaptability (whether bat response gene expression equalizes with viral yield as needed), and virus maintenance (how these higher yields and stronger responses affect viral shedding and transmission potential) and therefore warrants further exploration. Additionally, as previous data suggest that bat-to-bat transmission could occur through biting (i.e., subcutaneous inoculations in skin), future studies focused on the subcutaneous skin inoculation site are of particularly high biological relevance for understanding MARV replication and control in nature.^{5,6}

In conclusion, we hypothesize a refined model for disease tolerance to MARV infection in its bat reservoir. This model is defined by tissue-wide, moderate stimulation of canonical antiviral genes early in MARV infection, possibly relying on putative, noncanonical mechanisms (like IFN-independent induction) to finely calibrate a cluster of the innate immune response with rheostat-like precision. ERBs may thus have evolved to successfully disrupt viral replication without an evolutionary emphasis on adaptive responses for long-lived immunity or without triggering uncontrolled inflammatory gene expression responsible for the classical “cytokine storm” and subsequent severe immunopathology characterizing MARV disease in primates, including humans. Moving forward, it will be of paramount interest to elucidate the gene functions, molecular mechanisms, and immune cell types that mediate this disease tolerant phenotype following MARV infection, which may in turn be applicable to bat reservoir hosts of other emerging pathogens and translate into novel spillover control or antiviral therapeutic strategies that better protect humans from zoonotic viral infection and pathogenicity.

STAR★METHODS

Detailed methods are provided in the online version of this paper and include the following:

- **KEY RESOURCES TABLE**
- **RESOURCE AVAILABILITY**
 - Lead Contact
 - Materials Availability
 - Data and Code Availability
- **EXPERIMENTAL MODEL AND SUBJECT DETAILS**
- **METHOD DETAILS**
 - Biosafety
 - Viruses and antibodies
 - Inoculations and sampling
 - Euthanasia and necropsy
 - Cell preparation
 - Cell labeling and magnetic selection
 - Ex vivo CD14⁺ splenocyte infectivity assay
 - RNA isolation and TaqMan assay
 - nCounter hybridization and count detection
- **QUANTIFICATION AND STATISTICAL ANALYSIS**
 - ERB probe-based nCounter CodeSet
 - nCounter transcriptomic analysis
 - CIBERSORT analysis
 - Gene Ontology (GO) and pathway analysis

- Data visualization

SUPPLEMENTAL INFORMATION

Supplemental Information can be found online at <https://doi.org/10.1016/j.cub.2020.10.015>.

ACKNOWLEDGMENTS

The authors wish to thank Tatyana Klimova for her assistance with critical reading of the manuscript. Opinions, interpretations, conclusions, and recommendations are those of the authors and are not necessarily endorsed by the U.S. Army or the Centers for Disease Control and Prevention. This work was partially funded by the Defense Threat Reduction Agency, Department of Defense (HDTRA1-14-1-0016).

AUTHOR CONTRIBUTIONS

Conceptualization, J.S.T., G.F.P., M.S.-L., J.C.G., and J.B.P.; Experimentation, J.C.G., J.B.P., B.R.A., A.J.S., J.R.S., T.K.S., J.R.H., J.D.C.-M., and J.S.T.; Data Analysis, J.C.G., C.E.A., and J.B.P.; Funding Acquisition, G.F.P. and J.S.T.; Resources, K.A.K. and E.R.N.; Writing – Original Draft, J.C.G.; Review and Editing, J.C.G., J.S.T., M.S.-L., J.B.P., J.R.S., and R.K.

DECLARATION OF INTERESTS

The authors declare no competing interests.

Received: May 18, 2020

Revised: July 28, 2020

Accepted: October 7, 2020

Published: November 5, 2020

REFERENCES

1. Amman, B.R., Swanepoel, R., Nichol, S.T., and Towner, J.S. (2017). Ecology of Filoviruses. *Curr. Top. Microbiol. Immunol.* **411**, 23–61.
2. Towner, J.S., Pourrut, X., Albariño, C.G., Nkogue, C.N., Bird, B.H., Grard, G., Ksiazek, T.G., Gonzalez, J.P., Nichol, S.T., and Leroy, E.M. (2007). Marburg virus infection detected in a common African bat. *PLoS ONE* **2**, e764.
3. Jones, M.E., Schuh, A.J., Amman, B.R., Sealy, T.K., Zaki, S.R., Nichol, S.T., and Towner, J.S. (2015). Experimental Inoculation of Egyptian Roussette Bats (*Rousettus aegyptiacus*) with Viruses of the Ebolavirus and Marburgvirus Genera. *Viruses* **7**, 3420–3442.
4. Messaoudi, I., Amarasinghe, G.K., and Basler, C.F. (2015). Filovirus pathogenesis and immune evasion: insights from Ebola virus and Marburg virus. *Nat. Rev. Microbiol.* **13**, 663–676.
5. Schuh, A.J., Amman, B.R., Jones, M.E., Sealy, T.K., Uebelhoer, L.S., Spengler, J.R., Martin, B.E., Coleman-McCray, J.A., Nichol, S.T., and Towner, J.S. (2017). Modelling filovirus maintenance in nature by experimental transmission of Marburg virus between Egyptian roussette bats. *Nat. Commun.* **8**, 14446.
6. Amman, B.R., Jones, M.E., Sealy, T.K., Uebelhoer, L.S., Schuh, A.J., Bird, B.H., Coleman-McCray, J.D., Martin, B.E., Nichol, S.T., and Towner, J.S. (2015). Oral shedding of Marburg virus in experimentally infected Egyptian fruit bats (*Rousettus aegyptiacus*). *J. Wildl. Dis.* **51**, 113–124.
7. Hensley, L.E., Alves, D.A., Geisbert, J.B., Fritz, E.A., Reed, C., Larsen, T., and Geisbert, T.W. (2011). Pathogenesis of Marburg hemorrhagic fever in cynomolgus macaques. *J. Infect. Dis.* **204** (Suppl 3), S1021–S1031.
8. Fernando, L., Qiu, X., Melito, P.L., Williams, K.J., Feldmann, F., Feldmann, H., Jones, S.M., and Alimonti, J.B. (2015). Immune Response to Marburg Virus Angola Infection in Nonhuman Primates. *J. Infect. Dis.* **212** (Suppl 2), S234–S241.
9. Baker, M.L., Schountz, T., and Wang, L.F. (2013). Antiviral immune responses of bats: a review. *Zoonoses Public Health* **60**, 104–116.

10. Schountz, T., Baker, M.L., Butler, J., and Munster, V. (2017). Immunological Control of Viral Infections in Bats and the Emergence of Viruses Highly Pathogenic to Humans. *Front. Immunol.* **8**, 1098.
11. Brook, C.E., and Dobson, A.P. (2015). Bats as 'special' reservoirs for emerging zoonotic pathogens. *Trends Microbiol.* **23**, 172–180.
12. Zhou, P., Tachedjian, M., Wynne, J.W., Boyd, V., Cui, J., Smith, I., Cowled, C., Ng, J.H., Mok, L., Michalski, W.P., et al. (2016). Contraction of the type I IFN locus and unusual constitutive expression of IFN- α in bats. *Proc. Natl. Acad. Sci. USA* **113**, 2696–2701.
13. De La Cruz-Rivera, P.C., Kanchwala, M., Liang, H., Kumar, A., Wang, L.-F., Xing, C., and Schoggins, J.W. (2018). The IFN Response in Bats Displays Distinctive IFN-Stimulated Gene Expression Kinetics with Atypical RNASEL Induction. *J Immunol* **200**, 209–217.
14. McCarville, J.L., and Ayres, J.S. (2018). Disease tolerance: concept and mechanisms. *Curr. Opin. Immunol.* **50**, 88–93.
15. Hayman, D.T.S. (2019). Bat tolerance to viral infections. *Nat. Microbiol.* **4**, 728–729.
16. Mandl, J.N., Schneider, C., Schneider, D.S., and Baker, M.L. (2018). Going to Bat(s) for Studies of Disease Tolerance. *Front. Immunol.* **9**, 2112.
17. Banerjee, A., Rapin, N., Bollinger, T., and Misra, V. (2017). Lack of inflammatory gene expression in bats: a unique role for a transcription repressor. *Sci. Rep.* **7**, 2232.
18. Pavlovich, S.S., Lovett, S.P., Koroleva, G., Guito, J.C., Arnold, C.E., Nagle, E.R., Kulcsar, K., Lee, A., Thibaud-Nissen, F., Hume, A.J., et al. (2018). The Egyptian Roussette Genome Reveals Unexpected Features of Bat Antiviral Immunity. *Cell* **173**, 1098–1110.e18.
19. Arnold, C.E., Guito, J.C., Altamura, L.A., Lovett, S.P., Nagle, E.R., Palacios, G.F., Sanchez-Lockhart, M., and Towner, J.S. (2018). Transcriptomics Reveal Antiviral Gene Induction in the Egyptian Roussette Bat Is Antagonized In Vitro by Marburg Virus Infection. *Viruses* **10**, 607.
20. Lee, A.K., Kulcsar, K.A., Elliott, O., Khiabanian, H., Nagle, E.R., Jones, M.E., Amman, B.R., Sanchez-Lockhart, M., Towner, J.S., Palacios, G., and Rabadan, R. (2015). De novo transcriptome reconstruction and annotation of the Egyptian roussette bat. *BMC Genomics* **16**, 1033.
21. Prescott, J., Guito, J.C., Spengler, J.R., Arnold, C.E., Schuh, A.J., Amman, B.R., Sealy, T.K., Guerrero, L.W., Palacios, G.F., Sanchez-Lockhart, M., et al. (2019). Roussette Bat Dendritic Cells Overcome Marburg Virus-Mediated Antiviral Responses by Upregulation of Interferon-Related Genes While Downregulating Proinflammatory Disease Mediators. *MSphere* **4**, e00728-19.
22. Jones, M.E.B., Amman, B.R., Sealy, T.K., Uebelhoer, L.S., Schuh, A.J., Flietstra, T., Bird, B.H., Coleman-McCray, J.D., Zaki, S.R., Nichol, S.T., and Towner, J.S. (2019). Clinical, Histopathologic, and Immunohistochemical Characterization of Experimental Marburg Virus Infection in A Natural Reservoir Host, the Egyptian Roussette Bat (*Rousettus aegyptiacus*). *Viruses* **11**, 214.
23. Yen, B.C., and Basler, C.F. (2016). Effects of Filovirus Interferon Antagonists on Responses of Human Monocyte-Derived Dendritic Cells to RNA Virus Infection. *J. Virol.* **90**, 5108–5118.
24. Speranza, E., and Connor, J.H. (2017). Host Transcriptional Response to Ebola Virus Infection. *Vaccines (Basel)* **5**, 30.
25. Menicucci, A.R., Versteeg, K., Woolsey, C., Mire, C.E., Geisbert, J.B., Cross, R.W., Agans, K.N., Jankeel, A., Geisbert, T.W., and Messaoudi, I. (2017). Transcriptome Analysis of Circulating Immune Cell Subsets Highlight the Role of Monocytes in Zaire Ebola Virus Makona Pathogenesis. *Front. Immunol.* **8**, 1372.
26. Albariño, C.G., Uebelhoer, L.S., Vincent, J.P., Khristova, M.L., Chakrabarti, A.K., McElroy, A., Nichol, S.T., and Towner, J.S. (2013). Development of a reverse genetics system to generate recombinant Marburg virus derived from a bat isolate. *Virology* **446**, 230–237.
27. Fritz, E.A., Geisbert, J.B., Geisbert, T.W., Hensley, L.E., and Reed, D.S. (2008). Cellular immune response to Marburg virus infection in cynomolgus macaques. *Viral Immunol.* **21**, 355–363.
28. Cross, R.W., Speranza, E., Borisevich, V., Widen, S.G., Wood, T.G., Shim, R.S., Adams, R.D., Gerhardt, D.M., Bennett, R.S., Honko, A.N., et al. (2018). Comparative Transcriptomics in Ebola Makona-Infected Ferrets, Nonhuman Primates, and Humans. *J. Infect. Dis.* **278** (suppl_5), S486–S495.
29. Speranza, E., Altamura, L.A., Kulcsar, K., Bixler, S.L., Rossi, C.A., Schoepp, R.J., Nagle, E., Aguilar, W., Douglas, C.E., Delp, K.L., et al. (2017). Comparison of Transcriptomic Platforms for Analysis of Whole Blood from Ebola-Infected Cynomolgus Macaques. *Sci. Rep.* **7**, 14756.
30. Lin, K.L., Twenhafel, N.A., Connor, J.H., Cashman, K.A., Shamblin, J.D., Donnelly, G.C., Esham, H.L., Wlazlowski, C.B., Johnson, J.C., Honko, A.N., et al. (2015). Temporal Characterization of Marburg Virus Angola Infection following Aerosol Challenge in Rhesus Macaques. *J. Virol.* **89**, 9875–9885.
31. Connor, J.H., Yen, J., Caballero, I.S., Garamszegi, S., Malhotra, S., Lin, K., Hensley, L., and Goff, A.J. (2015). Transcriptional Profiling of the Immune Response to Marburg Virus Infection. *J. Virol.* **89**, 9865–9874.
32. Martínez Gómez, J.M., Periasamy, P., Dutertre, C.A., Irving, A.T., Ng, J.H., Cramer, G., Baker, M.L., Ginhoux, F., Wang, L.F., and Alonso, S. (2016). Phenotypic and functional characterization of the major lymphocyte populations in the fruit-eating bat *Pteropus alecto*. *Sci. Rep.* **6**, 37796.
33. Neumann, B., Klippert, A., Raue, K., Sopper, S., and Stahl-Hennig, C. (2015). Characterization of B and plasma cells in blood, bone marrow, and secondary lymphoid organs of rhesus macaques by multicolor flow cytometry. *J. Leukoc. Biol.* **97**, 19–30.
34. Periasamy, P., Hutchinson, P.E., Chen, J., Bonne, I., Shahul Hameed, S.S., Selvam, P., Hey, Y.Y., Fink, K., Irving, A.T., Dutertre, C.A., et al. (2019). Studies on B Cells in the Fruit-Eating Black Flying Fox (*Pteropus alecto*). *Front. Immunol.* **10**, 489.
35. Schnell, M.A., Zhang, Y., Tazelaar, J., Gao, G.P., Yu, Q.C., Qian, R., Chen, S.J., Varnavski, A.N., LeClair, C., Raper, S.E., and Wilson, J.M. (2001). Activation of innate immunity in nonhuman primates following intraportal administration of adenoviral vectors. *Mol. Ther.* **3**, 708–722.
36. Albariño, C.G., Wiggleton Guerrero, L., Lo, M.K., Nichol, S.T., and Towner, J.S. (2015). Development of a reverse genetics system to generate a recombinant Ebola virus Makona expressing a green fluorescent protein. *Virology* **484**, 259–264.
37. Albariño, C.G., Wiggleton Guerrero, L., Chakrabarti, A.K., and Nichol, S.T. (2018). Transcriptional analysis of viral mRNAs reveals common transcription patterns in cells infected by five different filoviruses. *PLoS ONE* **13**, e0201827.
38. Shaw, A.E., Hughes, J., Gu, Q., Behdenna, A., Singer, J.B., Dennis, T., Orton, R.J., Varela, M., Gifford, R.J., Wilson, S.J., and Palmarini, M. (2017). Fundamental properties of the mammalian innate immune system revealed by multispecies comparison of type I interferon responses. *PLoS Biol.* **15**, e2004086.
39. Caballero, I.S., Honko, A.N., Gire, S.K., Winnicki, S.M., Melé, M., Gerhardinger, C., Lin, A.E., Rinn, J.L., Sabeti, P.C., Hensley, L.E., and Connor, J.H. (2016). In vivo Ebola virus infection leads to a strong innate response in circulating immune cells. *BMC Genomics* **17**, 707.
40. Hume, A., and Mühlberger, E. (2018). Marburg Virus Viral Protein 35 Inhibits Protein Kinase R Activation in a Cell Type-Specific Manner. *J. Infect. Dis.* **278** (suppl_5), S403–S408.
41. Ashley, C.L., Abendroth, A., McSharry, B.P., and Slobedman, B. (2019). Interferon-Independent Innate Responses to Cytomegalovirus. *Front. Immunol.* **10**, 2751.
42. Ashley, C.L., Abendroth, A., McSharry, B.P., and Slobedman, B. (2019). Interferon-Independent Upregulation of Interferon-Stimulated Genes during Human Cytomegalovirus Infection is Dependent on IRF3 Expression. *Viruses* **11**, 246.
43. Schuh, A.J., Amman, B.R., Sealy, T.K., Kainulainen, M.H., Chakrabarti, A.K., Guerrero, L.W., Nichol, S.T., Albariño, C.G., and Towner, J.S. (2019). Antibody-Mediated Virus Neutralization Is Not a Universal

- Mechanism of Marburg, Ebola, or Sosuga Virus Clearance in Egyptian Rousette Bats. *J. Infect. Dis.* *219*, 1716–1721.
44. Storm, N., Jansen Van Vuren, P., Markotter, W., and Paweska, J.T. (2018). Antibody Responses to Marburg Virus in Egyptian Rousette Bats and Their Role in Protection against Infection. *Viruses* *10*, 73.
 45. Guivier, E., Galan, M., Salvador, A.R., Xuéreb, A., Chaval, Y., Olsson, G.E., Essbauer, S., Henttonen, H., Voutilainen, L., Cosson, J.F., and Charbonnel, N. (2010). Tnf- α expression and promoter sequences reflect the balance of tolerance/resistance to Puumala hantavirus infection in European bank vole populations. *Infect. Genet. Evol.* *10*, 1208–1217.
 46. Dubois, A., Castel, G., Murri, S., Pulido, C., Pons, J.B., Benoit, L., Loiseau, A., Lakhdar, L., Galan, M., Charbonnel, N., and Marianneau, P. (2017). Experimental infections of wild bank voles (*Myodes glareolus*) from nephropatia epidemica endemic and non-endemic regions revealed slight differences in Puumala virological course and immunological responses. *Virus Res.* *235*, 67–72.
 47. Easterbrook, J.D., and Klein, S.L. (2008). Seoul virus enhances regulatory and reduces proinflammatory responses in male Norway rats. *J. Med. Virol.* *80*, 1308–1318.
 48. Schountz, T., Acuña-Retamar, M., Feinstein, S., Prescott, J., Torres-Perez, F., Podell, B., Peters, S., Ye, C., Black, W.C., 4th, and Hjelle, B. (2012). Kinetics of immune responses in deer mice experimentally infected with Sin Nombre virus. *J. Virol.* *86*, 10015–10027.
 49. Srithayakumar, V., Sribalachandran, H., Rosatte, R., Nadin-Davis, S.A., and Kyle, C.J. (2014). Innate immune responses in raccoons after raccoon rabies virus infection. *J. Gen. Virol.* *95*, 16–25.
 50. Helin, A.S., Wille, M., Atterby, C., Järhult, J.D., Waldenström, J., and Chapman, J.R. (2018). A rapid and transient innate immune response to avian influenza infection in mallards. *Mol. Immunol.* *95*, 64–72.
 51. Munster, V.J., Adney, D.R., van Doremalen, N., Brown, V.R., Miazgowiec, K.L., Milne-Price, S., Bushmaker, T., Rosenke, R., Scott, D., Hawkinson, A., et al. (2016). Replication and shedding of MERS-CoV in Jamaican fruit bats (*Artibeus jamaicensis*). *Sci. Rep.* *6*, 21878.
 52. Woon, A.P., Boyd, V., Todd, S., Smith, I., Klein, R., Woodhouse, I.B., Riddell, S., Crameri, G., Bingham, J., Wang, L.F., et al. (2020). Acute experimental infection of bats and ferrets with Hendra virus: Insights into the early host response of the reservoir host and susceptible model species. *PLoS Pathog.* *16*, e1008412.
 53. Glennon, N.B., Jabado, O., Lo, M.K., and Shaw, M.L. (2015). Transcriptome Profiling of the Virus-Induced Innate Immune Response in *Pteropus vampyrus* and Its Attenuation by Nipah Virus Interferon Antagonist Functions. *J. Virol.* *89*, 7550–7566.
 54. Towner, J.S., Amman, B.R., Sealy, T.K., Carroll, S.A., Comer, J.A., Kemp, A., Swanepoel, R., Paddock, C.D., Balinandi, S., Khristova, M.L., et al. (2009). Isolation of genetically diverse Marburg viruses from Egyptian fruit bats. *PLoS Pathog.* *5*, e1000536.
 55. Huang, D.W., Sherman, B.T., and Lempicki, R.A. (2009). Systematic and integrative analysis of large gene lists using DAVID bioinformatics resources. *Nat. Protoc.* *4*, 44–57.
 56. Huang, D.W., Sherman, B.T., and Lempicki, R.A. (2009). Bioinformatics enrichment tools: paths toward the comprehensive functional analysis of large gene lists. *Nucleic Acids Res.* *37*, 1–13.
 57. Mi, H., Muruganujan, A., Ebert, D., Huang, X., and Thomas, P.D. (2019). PANTHER version 14: more genomes, a new PANTHER GO-slim and improvements in enrichment analysis tools. *Nucleic Acids Res.* *47* (D1), D419–D426.
 58. Luo, W., Pant, G., Bhavnasi, Y.K., Blanchard, S.G., Jr., and Brouwer, C. (2017). Pathview Web: user friendly pathway visualization and data integration. *Nucleic Acids Res.* *45* (W1), W501–W508.
 59. Heberle, H., Meirelles, G.V., da Silva, F.R., Telles, G.P., and Minghim, R. (2015). InteractiVenn: a web-based tool for the analysis of sets through Venn diagrams. *BMC Bioinformatics* *16*, 169.
 60. Glaze, E.R., Roy, M.J., Dalrymple, L.W., and Lanning, L.L. (2015). A Comparison of the Pathogenesis of Marburg Virus Disease in Humans and Nonhuman Primates and Evaluation of the Suitability of These Animal Models for Predicting Clinical Efficacy under the ‘Animal Rule’. *Comp. Med.* *65*, 241–259.
 61. Mire, C.E., Geisbert, J.B., Borisevich, V., Fenton, K.A., Agans, K.N., Flyak, A.I., Deer, D.J., Steinkellner, H., Bohorov, O., Bohorova, N., et al. (2017). Therapeutic treatment of Marburg and Ravn virus infection in nonhuman primates with a human monoclonal antibody. *Sci. Transl. Med.* *9*, eaai8711.

STAR★METHODS

KEY RESOURCES TABLE

REAGENT or RESOURCE	SOURCE	IDENTIFIER
Antibodies		
Rat monoclonal anti-CD14 (<i>Rousettus aegyptiacus</i> [ERB])	USAMRIID/Aldevron, LLC, Prescott et al. ²¹	N/A
Rat monoclonal anti-CD19 (ERB)	USAMRIID/Aldevron, Prescott et al. ²¹	N/A
Rat IgG-PE Isotype Control	Abcam	Cat#ab37368
Bacterial and Virus Strains		
MARV strain 371Bat2007	Albariño et al. ²⁶	GenBank: FJ750958.1
rMARV371-ZsG	Albariño et al. ^{36,37}	N/A
Biological Samples		
ERB tissue specimens	This paper	N/A
ERB splenocytes	This paper	N/A
ERB whole blood	This paper	N/A
ERB tissue-, cell- and blood-derived total RNA	This paper	N/A
Chemicals, Peptides, and Recombinant Proteins		
MagMAX RNA Lysis/Binding Solution Concentrate	Thermo Fisher Scientific	SKU#AM8500
Benzonase Nuclease HC, Purity > 90%	EMD Millipore	Cat#71205-3
ACK Lysing Buffer	GIBCO, Thermo	Cat#A1049201
LIVE/DEAD Fixable Aqua Dead Cell Stain Kit	Invitrogen, Thermo	Cat#L34966
autoMACS Rinsing Solution	Miltenyi Biotec	Cat#130-091-222
MACS® BSA Stock Solution	Miltenyi	Cat#130-091-376
Normal Rat Serum	Thermo	Cat#10710C
Anti-PE MicroBeads UltraPure	Miltenyi	Cat#130-105-639
Cytofix/Perm Buffer	BD Biosciences	Cat#554722
nCounter SPRINT Profiler Reagent Pack (including Hybridization Buffer)	NanoString	Cat# SPRINT-REAG-KIT
Critical Commercial Assays		
Lightning Link R-PE Conjugation Kit	Expedeon, Abcam	Cat#ab102918
Geno/Grinder 2000 Homogenizer	SPEX SamplePrep	N/A (Discontinued)
Spleen Dissociation Kit (mouse)	Miltenyi	Cat#130-095-926
gentleMACS Octo Dissociator with Heaters	Miltenyi	Cat#130-096-427
MACS MicroBead system w/ MultiMACS Cell24 Separator Plus	Miltenyi	Cat#130-098-637, Cat#130-095-691
MagMAX-96 Total RNA Isolation Kit (including TURBO DNase Buffer)	Applied Biosystems, Thermo	Cat#AM1830
MagMAX Pathogen RNA/DNA Kit	ABI, Thermo	Cat#4462359
SuperScript III Platinum One-Step qRT-PCR Kit	Thermo	Cat#11732088
nCounter Reporter ERB CodeSet	NanoString, Prescott et al. ²¹	N/A
nCounter Capture ERB ProbeSet	NanoString, Prescott et al. ²¹	N/A
nCounter SPRINT Cartridge	NanoString	Cat#SPRINT-CAR-1.0
Experimental Models: Organisms/Strains		
2 nd /3 rd gen captive-bred <i>R. aegyptiacus</i> bats (Uganda origin)	Amman et al. ⁶	N/A
Oligonucleotides		
MARV VP40 TaqMan F primer: GGA CCA CTG CTG GCC ATA TC	Amman et al. ⁶	N/A

(Continued on next page)

Continued

REAGENT or RESOURCE	SOURCE	IDENTIFIER
MARV VP40 TaqMan R primer: GAG AAC ATI TCG GCA GGA AG	Amman et al. ⁶	N/A
MARV VP40 TaqMan Marv Prb: /FAM/ ATC CTA AAC /ZEN/ AGG CTT GTC TTC TCT GGG ACT T /BkFQ/	Amman et al. ⁶	N/A
MARV VP40 TaqMan Ravv Prb: /FAM/ ATC CTG AAT /ZEN/ AAG CTC GTC TTC TCT GGG ACT T /BkFQ/	Amman et al. ⁶	N/A
Software and Algorithms		
FlowJo v10	FlowJo, LLC	https://www.flowjo.com/solutions/flowjo/downloads
7500 Software v2.0.6	Applied Biosystems, Thermo	https://www.thermofisher.com/us/en/home/technical-resources/software-downloads/applied-biosystems-7500-real-time-pcr-system.html
CIBERSORT	Stanford University	https://cibersort.stanford.edu/
nSolver v4.0 and nCounter Advanced Analysis Module v2.0.115	NanoString	https://www.nanostring.com/products/analysis-software/nsolver
GraphPad Prism v7.0 and v8.3.1	GraphPad Prism Software, Inc.	https://www.graphpad.com/scientific-software/prism/
DAVID v6.8	Huang et al. ^{55,56}	https://david.ncifcrf.gov/
PANTHER v14.1	Mi et al. ⁵⁷	http://www.pantherdb.org/
Ingenuity Pathway Analysis	QIAGEN Digital Insights	https://digitalinsights.qiagen.com/products-overview/discovery-insights-portfolio/analysis-and-visualization/qiagen-ipa/
Pathview Web	Luo et al. ⁵⁸	https://pathview.uncc.edu/
Morpheus	Broad Institute	https://software.broadinstitute.org/morpheus/
InteractiVenn	Heberle et al. ⁵⁹	http://www.interactivenn.net/

RESOURCE AVAILABILITY

Lead Contact

Further information and resource requests should be directed to and will be fulfilled by the Lead Contact, Jonathan S. Towner (jit8@cdc.gov).

Materials Availability

This study did not produce new unique reagents.

Data and Code Availability

The published article includes all datasets analyzed during the study (see [Data S1](#) and [S2](#)).

EXPERIMENTAL MODEL AND SUBJECT DETAILS

Work with 2nd- and 3rd-generation, captive-born ERBs (*Rousettus aegyptiacus*) from our colony of bats originally imported from Uganda was approved by the Centers for Disease Control and Prevention (CDC) Institutional Care and Use Committee (IACUC) in conjunction with the Animal Care and Use Review Office (ACURO) of the U.S. Army Medical Research and Materiel Command (USAMRMC). Work was conducted strictly following the Guide for the Care and Use of Laboratory Animals. CDC is accredited by the Association for Assessment and Accreditation of Laboratory Animal Care International (AAALAC). This study was a 28-day serial time course, conducted at biosafety level 4 (BSL-4) conditions, designed to investigate immune responses, via transcriptomic analysis, following inoculation of ERBs with MARV. 40 healthy juvenile (seven-month old) male and female ERBs were randomly assigned to one of eight cohorts, five bats per cohort. One cohort was euthanized 1, 2, 3, 5, 8, 13 (uninfected control bats), 14 and 28 days post-inoculation. ERBs were acclimated to the BSL-4 lab two weeks prior to inoculation. Each bat cohort was housed in cages in separate isolator units with HEPA-filtered inlet and exhaust air supplies (Duo-Flow Mobile Units, Lab Products, Inc. Seaford, DE, USA). Husbandry procedures were conducted daily, including housing in climate-controlled animal area within the BSL-4 lab, a 12 h day/night light cycle, routine animal room cleaning and animal observation, and daily provision of fresh fruit (body mass quantity) and water (*ad libitum*).^{3,6}

METHOD DETAILS

Biosafety

Work with infectious agents and infected animals was conducted at CDC (Atlanta, GA, USA) in a biological safety level 4 (BSL-4) laboratory in agreement with Select Agent protocols and practices (<https://www.selectagents.gov>). Researchers and animal care staff worked in accordance to BSL-4 level safety principles and adhered to proper infection control procedures to prevent cross contamination between bat cohorts. All animal handling was performed with leather bite gloves, with disposable latex gloves worn over the bite gloves when directly conducting animal procedures.

Viruses and antibodies

Inoculations were performed with MARV strain 371Bat2007 (GenBank: FJ750958.1), originally isolated from a naturally infected ERB caught at Kitaka Mine in Uganda in 2007 and passaged twice on Vero-E6 cells.²⁶ Separately, for *ex vivo* infection of CD14⁺ splenocytes from naive colony ERBs to validate monocyte infectivity, we used a recombinant version of MARV 371Bat2007 that expresses ZsGreen (rMARV371-ZsG), which acts as a marker of successful filoviral replication.^{21,26,36,37} ERB-specific monoclonal antibodies against CD14 and CD19 were custom-generated in partnership with USAMRIID. In brief, CD14 and CD19 target sequences were identified in the ERB genome and their extracellular domains cloned into a surface expression vector. This construct was sent to Aldevron, LLC (Fargo, ND, USA), where rats were immunized using a proprietary Genetic Immunization protocol. B cells from immunized rats were fused to generate hybridoma cells and further tested for reactivity toward either CD14 or CD19 using fast enzyme-linked immunosorbent assay (F-ELISA). For each target, the top 10 hybridomas were subcloned and retested using the same methodology. The top three hybridomas were sent to USAMRIID, where purified rat IgG from each hybridoma supernatant was pre-conjugated to various fluorophores via the Lightning Link Antibody Conjugation Kit system (Expedeon, Abcam, Cambridge, MA, USA) and further tested and optimized using *P. vampyrus* and ERB PBMCs by flow cytometry. The single top-performing monoclonal antibodies for CD14 and CD19 were selected by cell staining and plot profiling. Finally, prior to initiation of the bat study, the two validated antibodies were pre-conjugated to PE via the Lightning Link R-PE Kit.

Inoculations and sampling

Infections were performed as previously described in:^{3,6} under isoflurane anesthetic, bats were inoculated subcutaneously in the ventral abdomen with 10⁴ TCID₅₀ of MARV (250 μ L of 4 \times 10⁴/mL) in sterile Dulbecco's Modified Eagle's Medium (DMEM, GIBCO, Thermo Fisher Scientific, Waltham, MA, USA), while control bats were mock-inoculated with an equal volume of DMEM alone. This viral dosage, which is lethal in NHPs, has been shown to recapitulate the tissue tropism and viral load seen in natural ERB infections, including their lack of clinical disease, and is the inoculum our lab has adopted across several previous bat studies in order to maintain data consistency.^{5,6,60,61} To measure MARV RNA levels in whole blood over the course of the experiment, 20 μ L samples from each bat for RNA isolation were taken pre-inoculation, then daily post-inoculation until euthanasia, by venipuncture of the cephalic vein on the propatagium of alternating left/right wings using a sterile lancet (C&A Scientific, Manassas, VA, USA). Blood samples were placed directly into 130 μ L of 1 \times MagMAX RNA Lysis/Binding Solution (Applied Biosystems [ABI], Thermo) in a deep well plate.

Euthanasia and necropsy

Each bat cohort was euthanized under deep isoflurane anesthesia by exsanguination via cardiac puncture just under the xyphoid process, followed immediately by post-mortem necropsy. Tissues collected included liver, spleen, skin at the inoculation site and colon/rectum. Roughly 100mg tissue sections were collected for RNA isolation by placing them into 2mL grinding vials (OPS Diagnostics, Lebanon, NJ, USA) with 1mL of MagMAX RNA Lysis/Binding Solution Concentrate and homogenized for two minutes at 1500 strokes/min using a ball-mill tissue grinder (Geno/Grinder 2000, SPEX SamplePrep, Metuchen, NJ, USA). Additional spleen sections were processed into single-cell suspensions. Separately, naive colony bats were euthanized as above, and spleens harvested and processed for microscopy-based *ex vivo* validation of total splenocyte, CD14⁺ and CD19⁺ populations as well as rMARV371-ZsG infection of CD14⁺ splenocytes.

Cell preparation

Single-cell suspensions were produced by placing approximately half a spleen into a gentleMACS C tube (Miltenyi Biotec, Bergisch Gladbach, Germany), pre-loaded with 2.5mL Spleen Dissociation Kit (mouse) enzyme mix (Miltenyi) prepared according to manufacturer's instructions. Sealed C tubes were run on a gentleMACS Octo Dissociator with Heaters (program 37C_m_SDK_1). Roswell Park Memorial Institute (RPMI, GIBCO, Thermo) medium supplemented with 10% fetal bovine serum (FBS, HyClone, Cytiva Life Sciences, Marlborough, MA, USA), 1% Pen-Strep (GIBCO, Thermo) and 1:10000 Benzonase Nuclease HC (250U/ μ L, purity > 90%, EMD Millipore, Billerica, MA, USA) were added to cell suspensions, passed through 70 μ m strainers into conical tubes and spun at 350 \times g. Pellets were resuspended in ACK Lysing Buffer (GIBCO, Thermo) and incubated at room temperature with periodic inversion. Cells were washed and resuspended in RPMI/Benzonase, then enumerated using a MOXI Z Mini cell counter (ORFLO, Ketchum, ID, USA).

Cell labeling and magnetic selection

Splenocytes were subjected to 1) antibody labeling for flow cytometric validation; 2) enrichment for CD14⁺ or CD19⁺ cell populations via labeling and the magnetic-activated cell sorting (MACS) MicroBead system (Miltenyi) for RNA lysis; and 3) a combination of MACS

and flow validation, or microscopy-based validation of MACS-selected *ex vivo* samples from naive colony ERBs. For antibody labeling only, $\sim 1\text{--}2 \times 10^6$ splenocytes in 96-well round bottom plates were washed in Dulbecco's phosphate-buffered saline (D-PBS, Sigma-Aldrich, MilliporeSigma, St. Louis, MO, USA) and stained using the LIVE/DEAD Fixable Aqua Dead Cell Stain Kit (Invitrogen, Thermo). For MACS, up to 1×10^7 splenocytes in 96-well plates were washed in autoMACS buffer (MACS BSA Stock Solution diluted 1:20 in autoMACS Rinsing Solution, Miltenyi). For both procedures, cells were then blocked in D-PBS supplemented with 2% rat serum (D-PBS + RS, Thermo) prior to addition of D-PBS + RS containing CD14-PE or CD19-PE antibody. Labeled cells were washed and resuspended in D-PBS (for labeling alone) or, alternatively, washed in autoMACS buffer, incubated with anti-PE UltraPure MicroBeads and magnetically selected through 24-well column blocks in a MultiMACS Cell24 Separator Plus via either the POSSEL or POSSEL2 programs following manufacturer guidelines (Miltenyi). CD14⁺ and CD19⁺ splenocytes were then aliquoted for RNA lysis or flow analysis, while *ex vivo* total splenocytes or MACS-selected immune cells from naive colony ERBs were placed in 24-well plates and observed by microscopy using the EVOS FL Cell Imaging System (Thermo) after a one- or two-day incubation at 37°C to confirm cell morphology and homogeneity following MACS. Validation of labeling/MACS also included a rat IgG-PE isotype control (Abcam) and MACS negative fractions. Samples for flow cytometry were incubated in CytoFix/Perm buffer (BD Biosciences, San Jose, CA, USA) for at least 20 min. Prior to cytometric analysis, fixative was replaced with D-PBS + 2% FBS (STEMCELL Technologies Inc., Vancouver, BC, Canada). Samples were run on a Stratadigm S1000EX cytometer (San Jose, CA, USA) and data was analyzed using FlowJo version 10 (FlowJo, LLC, Ashland, OR, USA).

Ex vivo CD14⁺ splenocyte infectivity assay

CD14⁺ splenocytes from naive colony ERBs were placed into 5mL tubes, infected with rMARV371-ZsG at a multiplicity of infection of 0.5 and incubated at 37°C. After a 1 h adsorption, cells were spun and resuspended in fresh 10% RPMI + antibiotics, and then placed onto 24-well plates and re-incubated. ZsG fluorescence representing successful MARV replication in cells characteristic of monocytes/macrophages was visualized at D1, D2 and D3 by EVOS microscopy.

RNA isolation and TaqMan assay

Tissues, CD14⁺/CD19⁺ splenocytes and whole blood were lysed to inactivate virus using MagMAX RNA Lysis/Binding Solution with (blood and cells) or without (tissues) a 1:1 ratio with 100% isopropanol and removed from biocontainment. Total RNA was extracted by magnetic bead purification using either (for tissues) the MagMAX-96 Total RNA Isolation Kit with TURBO DNase treatment set for the AM1830_DW protocol or (for blood and cells) the MagMAX Pathogen RNA/DNA Kit (no DNase treatment) set for the AM1836_DW_50v2 (blood) or 4462359_DW_HV (cells) protocol, all run in a MagMAX Express-96 Deep Well Magnetic Particle Processor (ABI, Thermo). For tissues, each reaction used 125μL of lysate with 75μL of 100% isopropanol. RNA yield was assessed by NanoDrop (Thermo) as needed and stored at –80°C. Quantitative reverse-transcriptase polymerase chain reaction (qRT-PCR) of whole blood or liver/spleen was conducted using the SuperScript III Platinum One-Step qRT-PCR Kit (Thermo) via TaqMan primers/probes against MARV VP40 and run on an ABI 7500 Real-Time PCR System (Thermo) in tandem with 7500 Software v2.0.6. Relative TCID₅₀ equivalents per mL (blood) or g (tissues) were inferred from existing standard curves as described in,³ which were generated from ten-fold serial dilutions of MARV stocks used for bat inoculations that had been added to blood or tissue (calf liver) homogenate in the same manner as experimental samples.

nCounter hybridization and count detection

Hybridization reactions using a custom ERB-specific nCounter CodeSet (NanoString Technologies, Seattle, WA, USA) were performed on 12 samples per run according to manufacturer's instructions: 70μL hybridization buffer with or without RNase-free water was mixed with each Reporter CodeSet reagent, aliquoted into PCR tubes, mixed with up to 5μL, or in certain instances up to 8μL, of total RNA from ERB tissues or CD14⁺/CD19⁺ splenocytes, and finally mixed with each Capture ProbeSet reagent. Samples were pulse-spun, incubated for ~24 h at 65°C in a T100 thermal cycler (Bio-Rad, Hercules, CA, USA), re-spun, brought up to 32μL each with RNase-free water, mixed and 30μL loaded onto an nCounter cartridge for data collection using a SPRINT Profiler loaded with the BAT_IR_Panel_2_C6075 CodeSet Reporter Library File.

QUANTIFICATION AND STATISTICAL ANALYSIS

ERB probe-based nCounter CodeSet

A probe-based nCounter CodeSet targeting 380 ERB-specific immune genes, along with 10 probes targeting MARV (GenBank: FJ750958.1) transcripts, was designed under contract by NanoString using the Raegyp2.0 genome assembly (RefSeq: GCF_001466805.2) and the NCBI *R. aegyptiacus* Annotation Release 100 (Data S1 and S2).^{19,21} Following initial analyses, six genes showed ubiquitous borderline or below-background count threshold levels across tissue/cell datasets: *IFI44*, *IFITM2*, *IL12A*, *IL21*, *IL3* and *TLR9*. As differentiation between non-expression versus probe failure was not possible, these targets were removed from final analysis. IFN genes were exempted from exclusion due to known vagaries in IFN induction.

nCounter transcriptomic analysis

Data were processed by nSolver 4.0 (NanoString). After quality control of RCC files, raw counts in each complete dataset were normalized to geometric mean counts of synthetic positive controls (included in the CodeSet) to mitigate platform-based variation.

Due to failed quality control or positive controls, select bat samples were removed from analysis: bat #557 (control cohort) for liver, #906 (D1) for spleen, #509 (D2) for CD14⁺ splenocytes, and #139 (control) and #624 (D28) for colon. Using the nCAA module (version 2.0.115), the geNorm algorithm normalized each dataset by selecting the five most stable ERB genes as housekeepers. Housekeeper sets varied and are listed in [Data S1](#). nCAA computed DGE in the context of each complete dataset (using the “Optimal” setting) by comparing gene counts from infected bats at each time point to counts of corresponding genes from uninfected bats. Relevance, significance and count threshold criteria for DGE analysis at each time point were set to minimums of ± 2 FC, Benjamini-Yekutieli-adjusted p value ≤ 0.05 and above-background count threshold (i.e., genes deemed truly expressed) of $2 \times$ standard deviation (SD) of the mean count of all synthetic negative controls (included in the CodeSet) across all samples. All criteria were simultaneously required at one or more time point for a gene to be considered a bona fide DEG. For nCAA-based DGE analysis, only DEG values meeting these criteria were included in data visualization. Statistical information for DGE can further be found in figures and figure legends. For MARV quantification in skin, normalized viral gene or vRNA counts from each infected or control time point cohort were averaged and standard error assigned as noted in figures and figure legend; as bat #861 was the only animal with MARV gene and vRNA counts above background threshold in CD14⁺ splenocytes, averaging or standard error determination was not possible for this dataset. Count and DGE data can be found in [Data S1](#) and [S2](#) files.

CIBERSORT analysis

Normalized log₂ counts of all NanoString ERB CodeSet gene probes, for each tissue/cell type at each time point for each individual bat, were uploaded for analysis by web-based Cell-type Identification by Estimating Relative Subsets of RNA Transcripts (CIBERSORT, <https://cibersort.stanford.edu/>, Stanford University, Stanford, CA, USA). Analysis was run using a reference set of 22 immune cell subtypes (LM22) and run for 100 permutations. Cell subtypes were combined into the following general types: neutrophils, eosinophils, mast cells, dendritic cells, macrophages, monocytes, NK cells, T cells and B cells for graphing. Individual bats were averaged for each time point for summary graph figures. A two-tailed t test using individual bats as replicates was performed to determine statistical significance between cell types and time points as compared to uninfected (D13 NEG) control bats using GraphPad Prism (GraphPad Prism Software, Inc., La Jolla, CA, USA). Graphs were also created using Prism. Statistical information for CIBERSORT can further be found in related figures and figure legends where applicable.

Gene Ontology (GO) and pathway analysis

Functional annotation of all DEGs into general response networks was performed via GO analysis using both the web-based Database for Annotation, Visualization and Integrated Discovery (DAVID, <https://david.ncifcrf.gov/>, Frederick National Laboratory for Cancer Research, Frederick, MD, USA) and Protein Analysis Through Evolutionary Relationships (PANTHER, <http://www.pantherdb.org/>, University of Southern California, Los Angeles, CA, USA) programs.^{55–57} *Homo sapiens* was used as the annotation species. The GOTERM_BP_DIRECT was used to categorize genes via DAVID, while “GO biological process complete” was the annotation dataset employed by PANTHER, the latter of which had the Overrepresentation Test set as the analysis type (released on 07-11-2019) and the GO Ontology database set as the annotation version (released on 01-03-2020). Ingenuity Pathway Analysis (IPA, QIAGEN Digital Insights, Redwood City, CA, USA) was used to determine significantly enriched pathways and upstream regulators for each major tissue/cell dataset. DEGs and expression values with adjusted p values at each time point were uploaded and analyzed using “Core Analysis.” Comparison analysis was then performed across multiple time points for each tissue/cell type. The Ingenuity Knowledge Base was used to rank canonical pathways based on all species datasets and score them using a z-score algorithm that is calculated based upon uploaded dataset correlation with an activated state in that canonical pathway. P values were computed by IPA using a Fischer’s exact test to determine the probability that the association between the genes in the uploaded dataset and the genes in the canonical pathway are due to chance alone. Values obtained from IPA were graphed using Prism. Statistical information for IPA can further be found in related figures and figure legends. For Pathview Web analysis (<https://pathview.uncc.edu/>, University of North Carolina, Charlotte, NC, USA), Entrez Gene IDs corresponding to DEGs and log₂ FC were uploaded; KEGG diagrams were overlaid with gene changes.⁵⁸

Data visualization

Data were plotted using Microsoft Office Excel 2016, GraphPad Prism v7.0 and v8.3.1, Morpheus (<https://software.broadinstitute.org/morpheus/>, Broad Institute, Cambridge, MA, USA), InteractiVenn (<http://www.interactiVenn.net/>),⁵⁹ FlowJo v10.0, CIBERSORT, PANTHER v14.1, DAVID v6.8, IPA and Pathview Web. Related statistical information, where applicable, can be found in figures and figure legends.